MODELING OF RECTANGULAR COUNTER FLOW HEAT - RECIRCULATING COMBUSTOR

by

Bayındır Hüseyin SARACOĞLU

B.S.,Mechanical Engineering, Boğaziçi University, 2004

Submitted to the Institute for Graduate Studies in
Science and Engineering in partial fulfillment of
the requirements for the degree of
Master of Science

Graduate Program in Mechanical Engineering
Boğaziçi University

2008

ACKNOWLEDGEMENTS

First of all, I am grateful to my thesis supervisor Assoc. Prof. Hasan Bedir for his valuable support and guidance since the beginning of my academical studies.

I would like to thank all of my colleagues and my friends at the Mechanical Engineering Department of Bogazici University for their help and the good times we spent.

I am also grateful to all of my closest friend who have always been with me and supported me.

Last but not least, I would like to express my sincere gratitude to my family for their eternal support and encouragement on my thesis and my future decisions.

ABSTRACT

MODELING OF RECTANGULAR COUNTER FLOW HEAT - RECIRCULATING COMBUSTOR

The meso-scale, 3.5 turn Swiss-roll type counter flow heat recirculating combustor is modeled by a two dimensional finite-volume computational fluid dynamics (CFD) solver. The solver includes momentum, continuity, energy and *n-1* species equations solvers. The flow inside combustor is assumed to be steady and laminar. Thus, the simulations are made up to Reynolds number of 300. The structural material is INCONEL-718. Propane is burned with air. One step global chemical reaction is assumed for chemical modeling. The effects of Reynolds number and the equivalence ratio is investigated. An increasing trend in peak temperature with increasing Reynolds number is observed for the same equivalence ratio. Furthermore, the reaction zone moves upstream to the inlet. As the equivalence ratio increases the reaction zone broadens towards the inlet. The maximum temperatures increases as well. The decreasing wall thermal conductivity causes the lean extinction limit equivalence ratio to decrease.

ÖZET

DİKDÖRTGEN TERS AKIŞLI ISI - ÇEVİRİMLİ YANMA ODASI MODELLENMESİ

Mezo-boyutlu, 3.5 dönüşlü, Swiss Döngülü tip, ters akışlı, ısı geri dönüşümlü yanma odasi iki boyutlu sonlu hacimler sayısal akışkanlar dinamiği çözücüsü ile modellenmiştir. Çözücü momentum, süreklilik, enerji ve n-1 tane tür denklemi içermektedir. Yanma odası içerisindeki akış laminer ve zamana göre değişmez olarak kabul edilmiştir. Bu nedenle simulasyonlar belli Reynolds sayısına kadar yapılmıştır. Yapı malzemesi INCONEL-718'dir. Propan hava ile yakılmştır. Kimyasal modellemede tek adımlı genel kimyasal tepkime kabul edilmiştir. Reynolds sayısı ve eşdeğerlilik oranı etkisi incelenmiştir. Aynı eşdeğerlilik oranı için artan Reynolds sayılarında en yüksek sıcaklıklarda artış gözlenmektedir. Buna ek olarak tepkime bölgesi girişe doğru geri hareket etmektedir. Eşdeğerlilik oranı arttıkça tepkime bölgesi giriş yönüne doğru genişlemektedir. En yüksek sıcaklık miktarı da artmaktadır. Duvar ısı geçirgenliğinin azalması tükenme sınırlarındaki eşdeğerlilik oranının azalmasına neden olmaktadır.

TABLE OF CONTENTS

LIST OF FIGURES

LIST OF TABLES

LIST OF SYMBOLS/ABBREVIATIONS

$A_{I,j}$	Cell face area of v-control volume
$A_{i,J}$	Cell face area of u-control volume
a_E	Coefficient of flow variable of east control volume in discretised flow equation
a_N	Coefficient of flow variable of north control volume in discretised flow equation
a_P	Coefficient of flow variable of central control volume in discretised flow equation
a_S	Coefficient of flow variable of south control volume in discretised flow equation
a_W	Coefficient of flow variable of west control volume in discretised flow equation
B_k	Pre-exponential constant of kth reaction
$b_{i,J}$	Source term of u-momentum equation
$b_{I,j}$	Source term of v-momentum equation
c_p	Specific heat for constant pressure
D	Diffusive conductance
$D_{i,j}$	Binary diffusion coefficient of ith species into jth species
$D_{i,mix}$	Binary diffusion coefficient of ith species into mixture of species
E_a	Activation energy
F	Convective mass flux
k	Thermal conductivity
Mw_i	Molecular weight of ith species
Pe	Peclet number
p	Pressure
$p^{'}$	Correction pressure
p^*	Guessed pressure
R^ϕ	Residual for transport equations
R^c	Residual for continuity equation

R_u	Universal gas constant
Re	Reynolds number
S_ϕ	Source term for transport equation
T	Temperature
u	Velocity on horizontal direction
u^*	Guessed u velocity
v	Velocity on vertical direction
v^*	Guessed v velocity
w	Reaction rate
X_i	Molar fraction of ith species
Y_i	Mass fraction of ith species
α_k	Temperature exponent in the reaction rate equation
Γ	Diffusive coefficient
$\Delta h^o_{f,i}$	Enthalpy of reaction for ith reaction
δx_u	Horizontal distance between centers of u-control volumes
δy_u	Vertical distance between centers of u-control volumes
δx_v	Horizontal distance between centers of v-control volumes
δy_v	Vertical distance between centers of v-control volumes
μ	Viscosity
$\nu^{"}$	Stoichiometric coeficient for species appearing as a product
$\nu^{'}$	Stoichiometric coeficient for species appearing as a reactant
ξ	Space variable
ρ	Density
ϕ	Flow variable, equivalence ratio
$\dot{\omega}_i$	Reaction rate term for species i
CV	Control volume
V	Volume

1. INTRODUCTION

Combustion can basically be defined as the chemical reaction of a fuel and an oxidizer which results with heat rejection to the environment under appropriate conditions. The energy stored in the chemical bonds of the fuel is released by the combustion reaction.

Combustion is a field of study that has effects on almost everything in the modern life. From the electricity supply of the households to the aircraft propulsion, uncountable number of operation depends on combustion technology. When one starts his car's engine, he actually starts a complex reaction of gasoline combustion in the combustion chambers of the engine. The most of the energy need of the human kind is satisfied by combustion of the fossil fuels. So this makes combustion a contemporary research field.

In many fields of technology, the sizes of the products are getting lower. Computer technology is the best example. Today a laptop computer or even a PDA can easily process a job which was processed by a computer as large as a factory building forty years ago. This is the result of advances in micro and nano technology. The tendency of micro technology not only influences the electronics but also the field of mechanics. The MEMS (Micro Electro-Mechanic Systems) are begun to be developed by many research societies.

The MEMS - based devices are highly common in the appliances which are used in daily life. From the accelerometer in airbag control system of a car to the hard disk drive of a laptop computer, the MEMS - based components are so integrated to the wide spread gadgets, although people don't see them, they always work underneath.

These devices are widely powered by batteries. But for long time uninterrupted usage of the devices, the batteries couldn't supply enough energy. The power density of lithium- ion batteries is quite low than a hydrocarbon fuel. So this brings the micro

power generation issue together with micro combustors to the mind. Hydrocarbon fuels contain 100 times more energy per unit mass than lithium - ion batteries.[1] Methane, for instance, has power density of 10.9 MJ/kg , whereas a lithium - ion battery power density is 0.45 MJ/kg if the conversion efficiency of fuel chemical energy to electricity is assumed as 20%[2].

However, the micro-scale combustion brings many problems together with its advantages. The surface area to volume ratio increases as the scale of the combustor decreases. In other words the ratio of heat generation to the heat loss decreases with the size of the combustor. That makes harder to sustain and stabilize the flame in the combustor. Due to heat loss to the cold boundaries, the flame propagation is observed only within a region which is a characteristic distance much far from the boundaries. The distance is called quenching distance. As the length scale of the combustor gets closer to the quenching distance length scale, it gets harder to sustain the flame inside the combustor. So the cold boundary temperature becomes more important in micro scale. This problem may be solved either by heating the cold boundaries or switching the nature of combustion from gas phase to catalytic combustion or by using both approaches.

When all of the conditions stated above are considered together, the "Swiss Roll" excess enthalpy type combustor may be an appropriate power producing device for MEMS applications. This type of counter - flow burners recirculate the excess enthalpy of the combustion products stream to the reactants stream without mass transfer. So the combustion is sustained inside a region without extinguishment. The cold reactant stream is heated up during its way to combustion region without dilution. The catalysis can be deposited on the walls of the combustion chamber in order to have a catalytic combustion in addition to gas phase combustion.

1.1. Literature Survey

The interest in heat - recirculating "excess enthalpy" burners started with the studies of Lloyd, Weinberg and Jones [3, 4, 5] more than 30 years ago. In their re-

searches, the heat recirculating burners were studied in order to burn very lean mixture which couldn't be burned by conventional means and reduce the amount of pollutant emission of the combustion reactions. For a "Swiss Roll" type burner which has 0.4 cm by 3.5 cm flow channels, the experimental flammability limits are obtained for a very lean mixture of methane[3].

The thermodynamic model is constructed for a spiral counter current excess enthalpy burner is stated by Lloyd et al.[4] The temperatures at some locations and the losses inside combustor are formulated for the "Swiss Roll" combustor and the thermodynamic efficiency of the combustor is calculated. The experimental data are also collected in the study. According to their study, it is stated that having gone 82% of the way from the normal limit of flammability towards pure air, they discontinue the experiment and concluded that for all practical purpose there are no limits of flammability for combustion, when heat circulation is not accompanied by simultaneous dilution of the reactants with products.

The effect of heat recirculation in a combustor to expand the flammability limits of a mixture is stated by using global energy balance in the models of Jones et al.[5] Although the model consists of global heat generation, recirculation and loss to interpret the extinction limits, it is primitive to obtain quantitative achievements.

The first solid model is stated by Ronney[1]. For a counter - flow heat - recirculating combustor, the heat transfer from product stream to the reactant stream, and the heat loss to the ambient and conduction through the dividing wall is included in the model. It is stated that the stream - wise conduction through the dividing wall is a significant factor on extinction limit of the flame.

The experiments conducted by Ahn et al [6] show the characteristics of heat - recirculating "Swiss Roll" square meso-scale (where the length scale of the medium is comparable with quenching distance, burners with the dimensions of 7 cm by 7 cm by 5 cm). The channel height of the combustor is 3.5 mm. The study investigates the extinction limits of the burner for gas - phase and catalytic combustion modes, burner

temperatures. It showed that the presence of the platinum catalyst broadened the extinction limits in both lean and rich boundaries. The behavior of extinction limit according to the Reynolds numbers was also given in the study. The gas chromatography results of the exhaust gas for various setups were tabulated in the paper as well. The presence of fuel (C_3H_8)and other types of hydrocarbons, CO_2 and CO in the exhaust stream is measured over a region of equivalence ratios (from 0.45 to 8.78) and over a region of Reynolds number (from 10 to 1000) for catalytic and gas - phase combustion modes.

Chen and Buckmaster [7] propose a 2D model for "Swiss Roll" micro - scale combustor. In their model the combustor geometry is unwrapped in a straight tube in the middle of which combustion occurs. The original combustor has a rectangular geometry as in Ahn's experimental setup [6]. The heat diffusion from the walls, chemical reaction and heat transfer are considered in the model. The governing equations are non-dimensionalized. The coupled equations are solved. The unwrapped geometry has some gaps at the inner wall section. The sections of corners are compensated by filler where heat sources assumed.

The model created by Chen et al reproduced the experimental extinction limit of fuel - lean propane - air mixture for a channel height of 3.5 mm. The parametric studies is made over a range of Reynolds number, equivalence ratio, wall thermal conductivity and wall emissivity. The numerical result of extinction limit for channel heights of 1 mm and 0.5 mm were also obtained. As a result of the paper, while Reynolds number or equivalence ratio increases, the reaction rate increases and the flame front moves away form the center towards the inlet. The emissivity has an important role on the extinction limit for both low and high Reynold numbers, as well. The paper states that extinction limit increases almost linearly with increasing emissivity.

Another experimental study was made by Sitzki et al[8]. The 2D (a linearly extruded spiral shape) and 3D (Six wedge - shaped and torus shaped) "Swiss Roll" models were constructed. The combustors have 0.4 mm channel and 1 mm combustion chamber dimension. The catalyst strips made of nickel, palladium and copper plated

by platinum are placed in the combustion region. The fuels used in the experiments are propane and butane. In the study the Reynolds number (inlet velocity) and presence of catalysis inside the combustion chamber change the flammability limits in both ways. It stated that the flameless combustion mode was prevalent even without catalyst. With catalyst, the extinction limits narrow at higher Reynolds numbers but broaden substantially at lower Reynolds numbers, which are the conditions most relevant to micro scale combustion.

The experimental study of Kim et al [9] investigates the combustion characteristics of propane - air mixture in three different kinds of circular "Swiss roll" combustors at 5 different setups. In the paper, the channel depth (6 mm and 15 mm), the number of the channel turns (3 and 4), height of the channel (16mm and 27 mm) and combustion chamber width (3.5 mm and 12.7 mm) has been changed in order to find out the combustion behavior of the circular "Swiss roll" burners. No catalyst has been deposited on the surface of the combustion room. The gas phase reaction has been observed for different equivalence ratios and mean velocities. For some experimental setups the combustion reaction is observed by the help of the quartz cap on top of the "Swiss roll" burners. The surface temperatures of some location inside the combustor have been measured in order to find out the relation between the mean velocities of the gas stream and temperature inside the combustor.

Vican et al [10] introduced a micro reactor based on "Swiss roll" combustion chamber. The study involves power generation inside a micro reaction of dimension of 12.5 X 12.5 X 5.0 mm. The operation fuel is hydrogen in the experiments. The burning behavior of hydrogen - air mixtures of equivalence ratios of 0.2 to 1.0 is observed. A layer of catalyst (platinum) is deposited inside channels of "Swiss roll" in order to reduce the range of operating temperatures. An analytical model is tried to develop the burning behavior of the combustor. The model is compared with the experimental data. The changes in temperature with respect to equivalence ratios are measured. In addition, the observed temperatures in the catalytic surface reactions and gas - phase reactions are compared. The average combustor surface temperature of the gas phase combustion setups are around 600 K, whereas in catalytic combustion it is as low as

350 K.

The current research aims to investigate numerically the flow field, temperature field, reaction zone and species distribution in a rectangular "Swiss roll" combustor. The combustor is directly modeled without any geometrical simplification. The results are verified with the results in the literature for the combustor of the same size.The effects of inlet Reynolds number, reactant composition and wall thermal conductivity is studied. The changes in the reaction zone and temperature field is observed by changing the inlet mass flow and composition of the reactant stream. The effect of decreasing wall thermal conductivity on the lean extinction limit is analyzed.

2. MATHEMATICAL MODEL

2.1. Definition of the Problem

The model Swiss roll combustor has dimensions of 7 cm by 7 cm. It has solid walls separating the fuel -air mixture and the products of the combustion process.

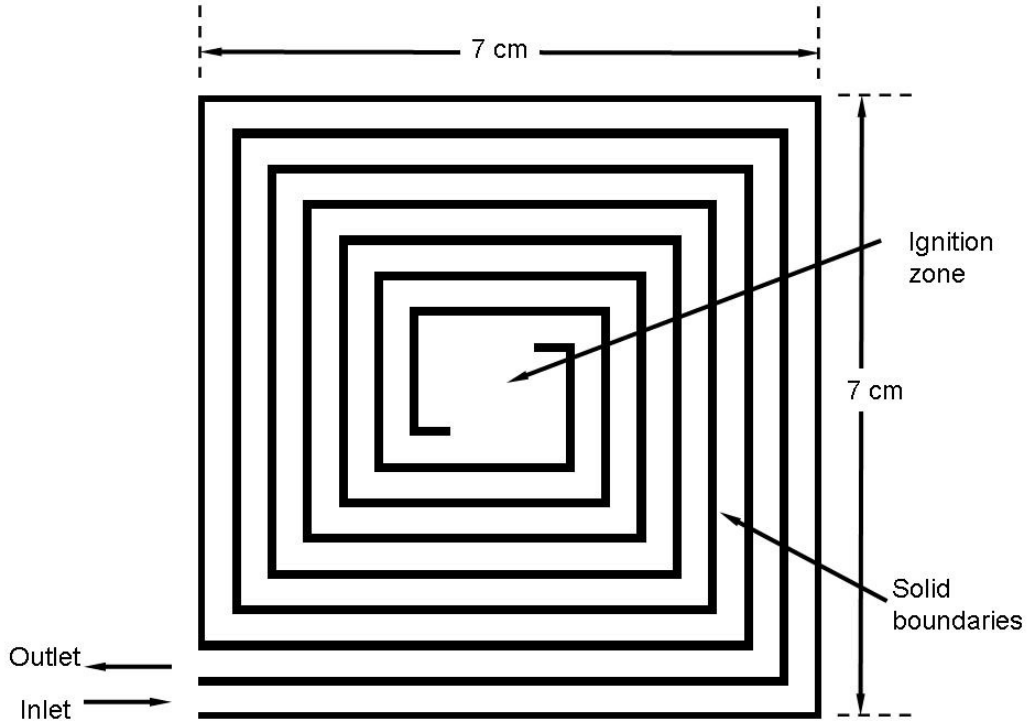

Figure 2.1. The Swiss roll geometry with 7 cm height and 7 cm width

The mixture of fuel and air with various fuel air ratios and at ambient temperature enter to the combustor with certain Reynolds numbers. The fuel-air mixture burns inside the combustion chamber. Finally, the mixture of products and reactants flows out of the combustion chamber through the outlet plug at certain temperature and composition. The flow entering to the combustor changes its direction several times due to the turning of the flow channel. Therefore, definition of the flow field is necessary. The mixture burns inside the reactor consequently the composition of mixture changes at the locations where the chemical reaction occurs. The transport of different species

in the mixture should be monitored for the reactants and the products of combustion. As a result of combustion, a particular amount of heat is released from the reaction zone. The heat is conducted and convected inside the fluid and conducted from hot products to the cold fresh reactant stream through the solid borders. This requires the investigation of the heat transfer phenomena together with fluid-solid conjugate heat transfer.

2.2. General Assumptions & Simplifications

A series of assumptions are needed to be set before attacking the solution of the problem defined. They are listed below.

- The problem is assumed to be *steady*:
- The problem is modeled as *two dimensional*:
- The flow assumed to be compressible.
- Viscosity of the flow is assumed to be constant.
- Conductivities of the fluid and the solid are assumed to be constant.
- Specific heat of the fluid and the solid are assumed to be constant.
- Binary diffusion coefficient of the individual species assumed to be constant.
- The effect of gravity is neglected.
- One step global reaction mechanism is studied.
- Radiative heat transfer mode is neglected.
- Viscous dissipation is neglected.
- Pressure heating effect is neglected.
- Soret and Duffor effects are neglected.

2.3. Governing Equations

- **Continuity Equation:** Steady, two dimensional continuity equation

$$\frac{\partial(\rho u)}{\partial x} + \frac{\partial(\rho v)}{\partial y} = 0 \tag{2.1}$$

where

u: horizontal component of velocity

v: vertical component of velocity

ρ: density

- **Species Mass Continuity Equation:** Steady, two dimensional species mass continuity equation

$$\frac{\partial(\rho u Y_i)}{\partial x} + \frac{\partial(\rho v Y_i)}{\partial y} = \frac{\partial}{\partial x}\left(\rho D \frac{\partial Y_i}{\partial x}\right) + \frac{\partial}{\partial y}\left(\rho D \frac{\partial Y_i}{\partial y}\right) + \dot{\omega}_i \tag{2.2}$$

where

Y_i: mass fraction of the ith species

D: binary diffustion coefficient of the ith species to the mixture

$\dot{\omega}_i$: rate of creation or destruction of the mass of the ith species

- **Momentum Equation:** Steady, two dimensional momentum equations without the body forces (gravitational force etc.) in conservative form

- x–Component:

$$\left(\frac{\partial(\rho u u)}{\partial x} + \frac{\partial(\rho u v)}{\partial y}\right) = -\frac{\partial p}{\partial x} + \mu\left(\frac{4}{3}\frac{\partial^2 u}{\partial x^2} + \frac{\partial^2 u}{\partial y^2} + \frac{1}{3}\frac{\partial^2 v}{\partial x \partial y}\right) \tag{2.3}$$

- y–Component:

$$\left(\frac{\partial(\rho u v)}{\partial x} + \frac{\partial(\rho v v)}{\partial y}\right) = -\frac{\partial p}{\partial y} + \mu\left(\frac{4}{3}\frac{\partial^2 v}{\partial y^2} + \frac{\partial^2 v}{\partial x^2} + \frac{1}{3}\frac{\partial^2 u}{\partial y \partial x}\right) \tag{2.4}$$

where

p: dynamic pressure

μ: dynamic viscosity

- **Energy Equation:** Steady, two dimensional energy equations without viscous dissipation and pressure effects in conservative form

$$\left(\frac{\partial(\rho u T)}{\partial x} + \frac{\partial(\rho v T)}{\partial y}\right) = \frac{k}{c_p}\left(\frac{\partial^2 T}{\partial x^2} + \frac{\partial^2 T}{\partial y^2}\right) - \sum \dot{\omega} \Delta h^0_{f,i} \tag{2.5}$$

where

T: temperature

k: thermal conductivity

c_p: specific heat at constant pressure

$\dot{\omega}$: molar rate of destruction of the fuel

$\Delta h^0_{f,i}$: heat of combustion

- **Ideal Gas Equation:** The state equation for the problem is ideal gas equation formulated for multi-species mixtures

$$\begin{aligned} p &= \rho R_u T \sum_{i=1}^{N} \frac{Y_i}{Mw_i} \\ \rho &= \frac{p}{R_u T \sum_{i=1}^{N} \frac{Y_i}{Mw_i}} \quad [12] \end{aligned} \tag{2.6}$$

where

R_u: Universal gas constant

N: number of species

Mw_i: molecular weight of the ith species

2.4. Chemical Reaction

The combustion of propane in the problem is modeled with one step global reaction. The stoichiometric reaction is given below.

$$C_3H_8 \quad + \quad 5(O_2 \quad + \quad 3.76N_2) \longrightarrow 3CO_2 \quad + \quad 4H_2O \quad + \quad 18.8N_2$$

2.5. Reaction Rate

The reaction rate term in the energy equation, $\dot{\omega}$ with the unit of kmol/s, and in and the species mass continuity equations, $\dot{\omega}_i$ with the unit of kg/s, are calculated according to the equation 2.7 and 2.8 respectively after Westbrook and Dryer. The constants in the equation is also taken from their work [11].

$$\dot{\omega} = BT^{\alpha} \exp\left(-\frac{E_a}{R_u T}\right) \left(\frac{X_f p}{R_u T}\right)^a \left(\frac{X_o p}{R_u T}\right)^b \qquad [13] \qquad (2.7)$$

$$\dot{\omega}_i = Mw_i(\nu_i'' - \nu_i')BT^{\alpha} \exp\left(-\frac{E_a}{R_u T}\right) \left(\frac{X_f p}{R_u T}\right)^a \left(\frac{X_o p}{R_u T}\right)^b \qquad [12] \qquad (2.8)$$

where

B: Pre-exponential constant

α: temperature exponent

E_a: activation energy

X_f: molar fraction of the fuel

X_o: molar fraction of oxygen

a: exponent of fuel fraction

b: exponent of oxygen fraction

ν_i'': Stoichiometric coefficient of ith product

ν_i': Stoichiometric coefficient of ith reactant

Table 2.1. The values of the constants in the reaction rate expressions 2.7 and 2.8 for combustion of propane [14]

B	α	$E_a(kcal/kmol)$	$R_u(kcal/kmolK)$	p (Pa)	a	b
8.6×10^{10}	0	$30,000$	1.987	$101,325$	0.1	1.65

2.6. Material Properties

The material properties, namely thermal conductivity, specific heat, viscosity of the fluid mixture running inside the combustion chamber are assumed to be constant with changing temperature of the medium and set to be equal to $0.0242W/mK$, $1006.43J/kgK$ and $1.72 \times 10^{-}5kg/ms$ respectively. The binary diffusion coefficients of individual species are assumed to be equal to their values at *350 K* and tabulated in 2.2. However, binary diffusion coefficient of individual species to the mixture is calculated as a function of changing molar fractions of the species in the mixture according to the equation 2.9. Furthermore, the solid material is chosen as INCONEL-718. The properties of the solid is also assumed to be constant with respect to temperature. The thermal conductivity of INCONEL-718 is also assumed to be $11.4W/mK$ and specific heat is $435J/kgK$.

Table 2.2. The binary diffusion coefficients of reactants and products into each other for combustion of propane

$D_{ji}[cm^2/s]$	C_3H_8	O_2	CO_2	H_2O	N_2
C_3H_8	–	0.1529	0.1563	0.2977	0.1491
O_2	0.1529	–	0.2128	0.3103	0.2577
CO_2	0.1563	0.2128	–	0.2114	0.2015
H_2O	0.2977	0.3103	0.2114	–	0.2977
N_2	0.1491	0.2577	0.2015	0.2977	–

$$D_{i,m} = \frac{1 - X_i}{\sum_{j \neq i}^{K} \frac{X_j}{D_{ji}}} \qquad [15] \tag{2.9}$$

In equation 2.9, the binary diffusion coefficients $D_{i,m}$ and D_{ji} designate binary diffusion coefficient of ith species into the mixture and binary diffusion coefficient of jth species into ith species.

2.7. Boundary Conditions

2.7.1. Momentum Equations

There are several boundary condition for the problem regarding the governing equation. At the inlet port of the reactor which is shown in figure 2.1, a *Dirichlet* type boundary condition is used to specify flow velocity at the inlet in both horizontal and vertical directions. On the solid reactor walls, no-slip (*Dirichlet*) wall boundary conditions are imposed for the flow equations. For no-slip boundary conditions, the flow velocity which is parallel to the solid wall is set to zero. At the outlet of the combustor, outflow boundary condition (*Neumann*) is imposed for not only the momentum equations but also energy and species mass continuity equations. This means that the flow properties at the exit of the boundary do not change on the flow direction as the exit is approached.

2.7.2. Energy Equation

The temperature of the flow entering to the combustor is set equal to the ambient temperature which is assumed as *300 K*. At the outermost solid boundaries, both adiabatic wall (*Neumann*) boundary condition and constant ambient temperature wall (*Dirichlet*) boundary conditions are used for different cases. The outflow boundary condition is applied at the flow exit location.

2.7.3. Species Mass Continuity Equation

The inlet composition of the reactant stream is given at the inlet boundary as a constant value (*Dirichlet*). At the flow exit port, outflow (*Neumann*) boundary condition is imposed. On the solid walls of the reactor, impermeable wall (*Neumann*)

boundary condition is imposed.

A summary of the boundary condition for all governing equations are given in figure 2.2 below.

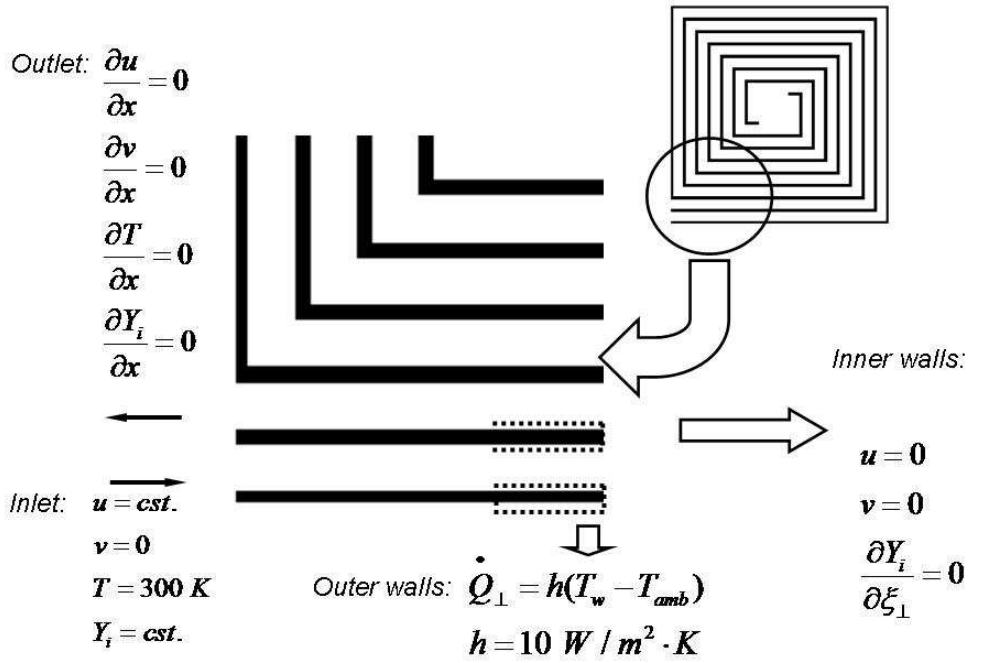

Figure 2.2. Boundary conditions of governing equations at different locations on the model

3. COMPUTATIONAL MODEL

3.1. Finite Volume Method

The governing equations of the system which are stated in chapter 2 should be converted into a set of algebraic equation in order to find the solution for the problem. For this purpose, finite volume approach is followed. The method is based on application of the differential equations on finite volumes in the domain of calculation. The steady differential equations which are going to be calculated are rearranged into the form in equation 3.2. The term in the differential equation can be classified as convective, diffusive and source terms.

$$\underbrace{div\,(\rho \mathbf{u}\phi)}_{Convective\ term} = \underbrace{div\,(\Gamma grad\phi)}_{Diffusive\ term} + \underbrace{S_\phi}_{Source\ term} \tag{3.1}$$

The equation in this form is integrated over a finite volume. Therefore the differential equation is converted to a integral equation as below.

$$\underbrace{\int_{\mathbf{A}} \mathbf{n}\cdot(\rho \mathbf{u}\phi)\,dA}_{Net\ convective\ flux} = \underbrace{\int_{\mathbf{A}} \mathbf{n}\cdot(\Gamma grad\phi)\,dA}_{Net\ diffusive\ flux} + \underbrace{\int_{\mathbf{CV}} S_\phi dV}_{Generation\ of\ \phi} \qquad [16] \tag{3.2}$$

3.2. Discretisation of the Governing Equations

The governing equations are needed to be discretised in order to end up with algebraic equations. After the governing equations are rewritten in the form of equation 3.2, the discretisation takes place. The general form of discretised equation equations

is stated in the equation 3.3.

$$a_P\phi_P = a_W\phi_W + a_E\phi_E + a_S\phi_S + a_N\phi_N + S_\phi \qquad [17] \qquad (3.3)$$

The coefficients (a's) are coefficients of variable of the differential equation when it is converted to an algebraic one. The subscripts designates the neighboring cells to the cell P where the equation is calculated. This notation can be better understood by the help of figure 3.1

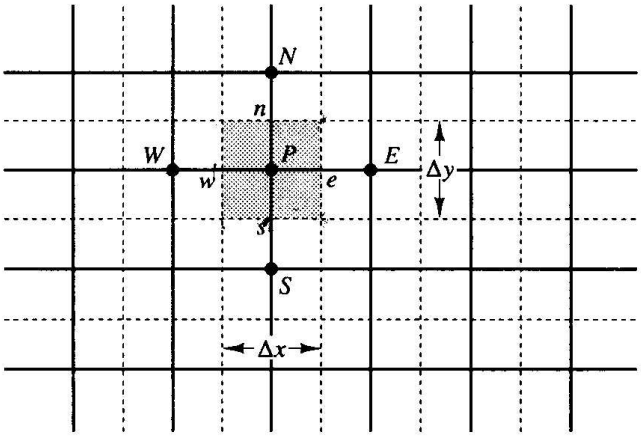

Figure 3.1. Finite volume cells in two dimensional grid[16]

When a convective-diffusive problem is considered, two variables are defined to have the discretisation formulation. Those are F and D. They represent convective mass flux per unit are and diffusion conductance at cell faces.

$$F = \rho u \text{ and } D = \frac{\Gamma}{\delta x} \qquad (3.4)$$

Those are used individually or in a combination in order to calculate the coefficient of the algebraic equations. Therefore a discretisation scheme is needed to be utilized.

In this work, all of the governing equations are discretised with hybrid differencing scheme.

3.2.1. The Hybrid Differencing Scheme

The hybrid scheme is a combination of central differencing scheme which is second order accurate and upwind differencing scheme which is first order accurate. The decision is made by the scheme based on magnitude of a dimensionless number which is called Peclet number (Pe). The non-dimensional cell Peclet number is a measure of the relative strengths of convection and diffusion[17]. It is calculated as in equation 3.5. If the diffusive strength is greater than the convective strength of the flow ($Pe < 2$), the central differencing is employed. Whereas, if the flow convective dominated ($Pe \geq 2$), the upwind scheme is used.

$$Pe = \frac{F}{D} = \frac{\rho u}{\Gamma/\delta x} \qquad [17] \tag{3.5}$$

where

F: Convective mass flux

D: Diffusive conductance

Γ: Diffusive coefficient

δx: Distance between centers of finite volumes

As the scheme is applied to convert a two dimensional differential equation in the form of equation 3.2 to the form stated in equation 3.3, the coefficients are computed as below:

$$a_W = max\left[F_w, \left(D_w + \frac{F_w}{2}\right), 0\right] \tag{3.6}$$

$$a_E = max\left[-F_e, \left(D_e - \frac{F_e}{2}\right), 0\right] \tag{3.7}$$

$$a_S = max\left[F_s, \left(D_s + \frac{F_s}{2}\right), 0\right] \tag{3.8}$$

$$a_N = max\left[-F_n, \left(D_n + \frac{F_n}{2}\right), 0\right] \tag{3.9}$$

$$a_P = a_W + a_E + a_S + a_N + \Delta F \tag{3.10}$$

$$\text{where } \Delta F = F_w - F_w + F_n - F_s$$

3.3. Discretised Governing Equations

3.3.1. Momentum equations

The momentum equations are discretised according to the considerations stated above. But there is one more thing to be considered for the momentum equations. That is the construction of the grid for the velocity components and the scalars, here the pressure. In order to sense the pressure changes and the effect on the momentum equations better, the staggered grid philosophy is followed in the calculations [16]. Therefore, the velocities are defined on the cell faces and the scalars are on the cell centers. So, there are three different grid system created in this case. These are one for the scalar quantities, one which is staggered to left for the horizontal velocity component and lastly one which is staggered down for vertical component of the velocity. The schematic of the staggered grid system is shown in figure 3.2.

The differential form of the momentum equations are given in the equations below together with continuity equation.

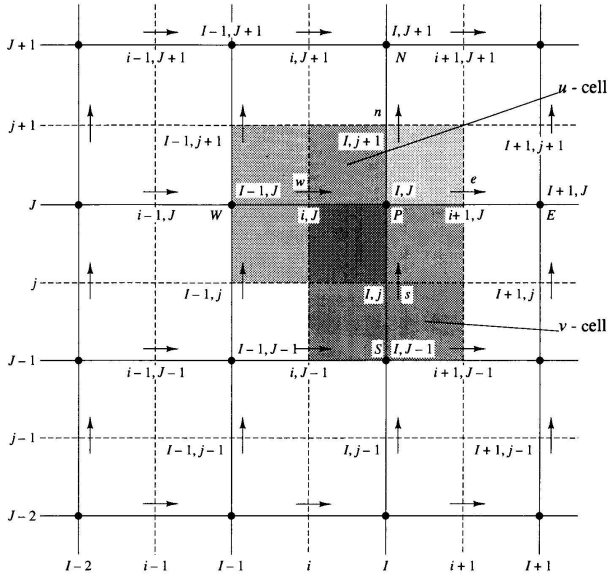

Figure 3.2. The staggered grid[16]

$$\underbrace{\frac{\partial}{\partial x}(\rho uu)+\frac{\partial}{\partial y}(\rho uv)}_{\text{Convective terms}}=\underbrace{\frac{\partial}{\partial x}\left[\mu\left(\frac{\partial u}{\partial x}\right)\right]+\frac{\partial}{\partial y}\left[\mu\left(\frac{\partial u}{\partial y}\right)\right]}_{\text{Diffusive terms}}\underbrace{-\frac{\partial p}{\partial x}}_{\text{Pressure gradient term}}\underbrace{\frac{1}{3}\frac{\partial}{\partial x}\left(\mu\frac{\partial u}{\partial x}\right)+\frac{\partial}{\partial y}\left(\mu\frac{\partial v}{\partial x}\right)-\frac{2}{3}\frac{\partial}{\partial x}\left(\mu\frac{\partial v}{\partial y}\right)}_{\text{The source term}} \tag{3.11}$$

$$\underbrace{\frac{\partial}{\partial x}(\rho uv)+\frac{\partial}{\partial y}(\rho vv)}_{\text{Convective terms}}=\underbrace{\frac{\partial}{\partial x}\left[\mu\left(\frac{\partial v}{\partial x}\right)\right]+\frac{\partial}{\partial y}\left[\mu\left(\frac{\partial v}{\partial y}\right)\right]}_{\text{Diffusive terms}}\underbrace{-\frac{\partial p}{\partial y}}_{\text{Pressure gradient term}}\underbrace{\frac{\partial}{\partial x}\left(\mu\frac{\partial u}{\partial y}\right)+\frac{1}{3}\frac{\partial}{\partial y}\left(\mu\frac{\partial v}{\partial y}\right)-\frac{2}{3}\frac{\partial}{\partial y}\left(\mu\frac{\partial u}{\partial x}\right)}_{\text{The source term}} \tag{3.12}$$

$$\frac{\partial(\rho u)}{\partial x}+\frac{\partial(\rho v)}{\partial y}=0 \tag{3.13}$$

The momentum equations are discretised in the form stated below.

x-momentum equation:

$$\begin{aligned} a_{i,J}u_{i,J} &= \sum a_{nb}u_{nb} - \frac{p_{I,J} - p_{I-1,J}}{\delta x_u}\Delta V_u + \overline{S_v}\Delta V_v \\ &\text{or} \\ a_{i,J}u_{i,J} &= \sum a_{nb}u_{nb} + \left(p_{I-1,J} - p_{I,J}\right) A_{i,J} + b_{i,J} \qquad [16] \end{aligned} \tag{3.14}$$

The source term of the x-momentum equation for compressible flow is stated in equation 3.15 and discretised form of the term is given in equation 3.15.

$$\begin{aligned} \overline{S_u}\Delta V_u &= \left[\frac{1}{3}\frac{\partial}{\partial x}\left(\mu\frac{\partial u}{\partial x}\right) + \frac{\partial}{\partial y}\left(\mu\frac{\partial v}{\partial x}\right) - \frac{2}{3}\frac{\partial}{\partial x}\left(\mu\frac{\partial v}{\partial y}\right)\right]_{cell} \cdot \Delta V_u \\ &= \left[\frac{1}{3}\frac{\left(\mu\frac{\partial u}{\partial x}\right)_{\text{east face}} - \left(\mu\frac{\partial u}{\partial x}\right)_{\text{west face}}}{\delta x_u} + \frac{\left(\mu\frac{\partial v}{\partial x}\right)_{\text{north face}} - \left(\mu\frac{\partial v}{\partial x}\right)_{\text{south face}}}{\delta y_u}\right. \\ &\quad \left. -\frac{2}{3}\frac{\left(\mu\frac{\partial v}{\partial y}\right)_{\text{east face}} - \left(\mu\frac{\partial v}{\partial y}\right)_{\text{west face}}}{\delta x_u}\right] \cdot \Delta V_u \\ \overline{S_u}\Delta V_u &= \left[\frac{1}{3}\frac{\left(\mu\frac{u_{i+1,J}-u_{i,J}}{\delta x_{PE}}\right) - \left(\mu\frac{u_{i,J}-u_{i-1,J}}{\delta x_{WP}}\right)}{\delta x_u} + \frac{\left(\mu\frac{v_{I,j+1}-v_{I-1,j+1}}{\delta x_u}\right) - \left(\mu\frac{v_{I,j}-v_{I-1,j}}{\delta x_u}\right)}{\delta y_u}\right. \\ &\quad \left. -\frac{2}{3}\frac{\left(\mu\frac{v_{I,j+1}-v_{I,j}}{\delta y_u}\right) - \left(\mu\frac{v_{I-1,j+1}-v_{I-1,j}}{\delta y_u}\right)}{\delta x_u}\right] \cdot \delta x_u \delta y_u \end{aligned} \tag{3.15}$$

y-momentum equation:

$$
\begin{aligned}
a_{I,j}v_{I,j} &= \sum a_{nb}v_{nb} - \frac{p_{I,J-1} - p_{I,J}}{\delta y_u}\Delta V_v + \overline{S_v}\Delta V_v \\
&\text{or} \\
a_{I,j}v_{I,j} &= \sum a_{nb}v_{nb} + \left(p_{I,J} - p_{I,J-1}\right) A_{I,j} + b_{I,j} \qquad [16] \qquad (3.16)
\end{aligned}
$$

The source term of the y-momentum equation for compressible flow is stated in equation 3.17 and discretised form of the term is given in equation 3.17.

$$
\begin{aligned}
\overline{S_v}\Delta V_v &= \left[\frac{\partial}{\partial x}\left(\mu\frac{\partial u}{\partial y}\right) + \frac{1}{3}\frac{\partial}{\partial y}\left(\mu\frac{\partial v}{\partial y}\right) - \frac{2}{3}\frac{\partial}{\partial y}\left(\mu\frac{\partial u}{\partial x}\right)\right]\cdot\Delta V_v \\
&= \left[\frac{\left(\mu\frac{\partial u}{\partial y}\right)_{\text{east face}} - \left(\mu\frac{\partial u}{\partial y}\right)_{\text{west face}}}{\delta x_v} + \frac{1}{3}\frac{\left(\mu\frac{\partial v}{\partial y}\right)_{\text{north face}} - \left(\mu\frac{\partial v}{\partial y}\right)_{\text{south face}}}{\delta y_v}\right. \\
&\quad \left. - \frac{2}{3}\frac{\left(\mu\frac{\partial u}{\partial x}\right)_{\text{north face}} - \left(\mu\frac{\partial u}{\partial x}\right)_{\text{south face}}}{\delta x_v}\right]\cdot\Delta V_v \\
\overline{S_v}\Delta V_v &= \left[\frac{\left(\mu\frac{u_{i+1,J}-u_{i+1,J-1}}{\delta y_v}\right) - \left(\mu\frac{u_{i,J}-u_{i,J-1}}{\delta y_v}\right)}{\delta x_v} + \frac{1}{3}\frac{\left(\mu\frac{v_{I,j+1}-v_{I,j}}{\delta y_{PN}}\right) - \left(\mu\frac{v_{I,j}-v_{I,j-1}}{\delta y_{SP}}\right)}{\delta y_v}\right. \\
&\quad \left. - \frac{2}{3}\frac{\left(\mu\frac{u_{i+1,J}-u_{i,J}}{\delta x_v}\right) - \left(\mu\frac{u_{i+1,J-1}-u_{i,J-1}}{\delta x_v}\right)}{\delta y_v}\right]\cdot\delta x_v\delta y_v \qquad (3.17)
\end{aligned}
$$

The continuity equation is discretised and coupled with the momentum equations by using a special algorithm which is called Semi-Implicit Method for Pressure Linked Equations (SIMPLE)[18]. The algorithm is explained in the next section.

3.3.1.1. Solution Algorithm - SIMPLE. The last equation of the flow which is continuity equation is discretised by using an algorithm which is originally developed by Patankar and Spalding[19]. The idea of the algorithm is to define correct pressure field as the sum of the guessed pressure field (p^*) and a correction pressure (p'). Therefore the same philosophy is applied to the correct velocity fields. After some algebra and an approximation the final discretised continuity equation is found in the equation 3.18 below.

$$a_{I,J}p'_{I,J} = a_{I+1,J}p'_{I+1,J} + a_{I-1,J}p'_{I-1,J} + a_{I,J+1}p'_{I,J+1} + a_{I,J-1}p'_{I,J-1} + b'_{I,J} \tag{3.18}$$

where

$$a_{I+1,J} = \left(\rho\frac{A}{a}A\right)_{i+1,J} \quad a_{I-1,J} = \left(\rho\frac{A}{a}A\right)_{i,J} \quad a_{I,J+1} = \left(\rho\frac{A}{a}A\right)_{I,j+1} \quad a_{I,J-1} = \left(\rho\frac{A}{a}A\right)_{I,j}$$

$$b'_{I,J} = (\rho u^* A)_{i,J} - (\rho u^* A)_{i+1,J} + (\rho u^* A)_{I,j} - (\rho u^* A)_{I,j-1}$$

The calculations start with an initial guess of primitive variables of the flow for all the domain. After the momentum equations are solved by those variables the new guess for the velocity field is obtained. This velocity field is corrected by the pressure correction terms as in equations below.

$$u'_{i,J} = d_{i,J}(p'_{I-1,J} - p'_{I,J}) \tag{3.19}$$

$$v'_{I,j} = d_{I,j}(p'_{I,J-1} - p'_{I,J}) \tag{3.20}$$

$$\text{where} \quad d_{i,J} = \frac{A_{i,J}}{a_{i,J}} \text{and} \quad d_{I,j} = \frac{A_{I,j}}{a_{I,j}}$$

These values are used in the pressure correction equation and the next the correct velocity and pressure field is calculated. Finally, the other scalar transport equations are solved. The last step is to check if the solution is converged. If it is not, the calculated field of vectors and scalar variables are used as an initial guess for the next iteration step. The block diagram of the SIMPLE algorithm is given in figure 3.3.

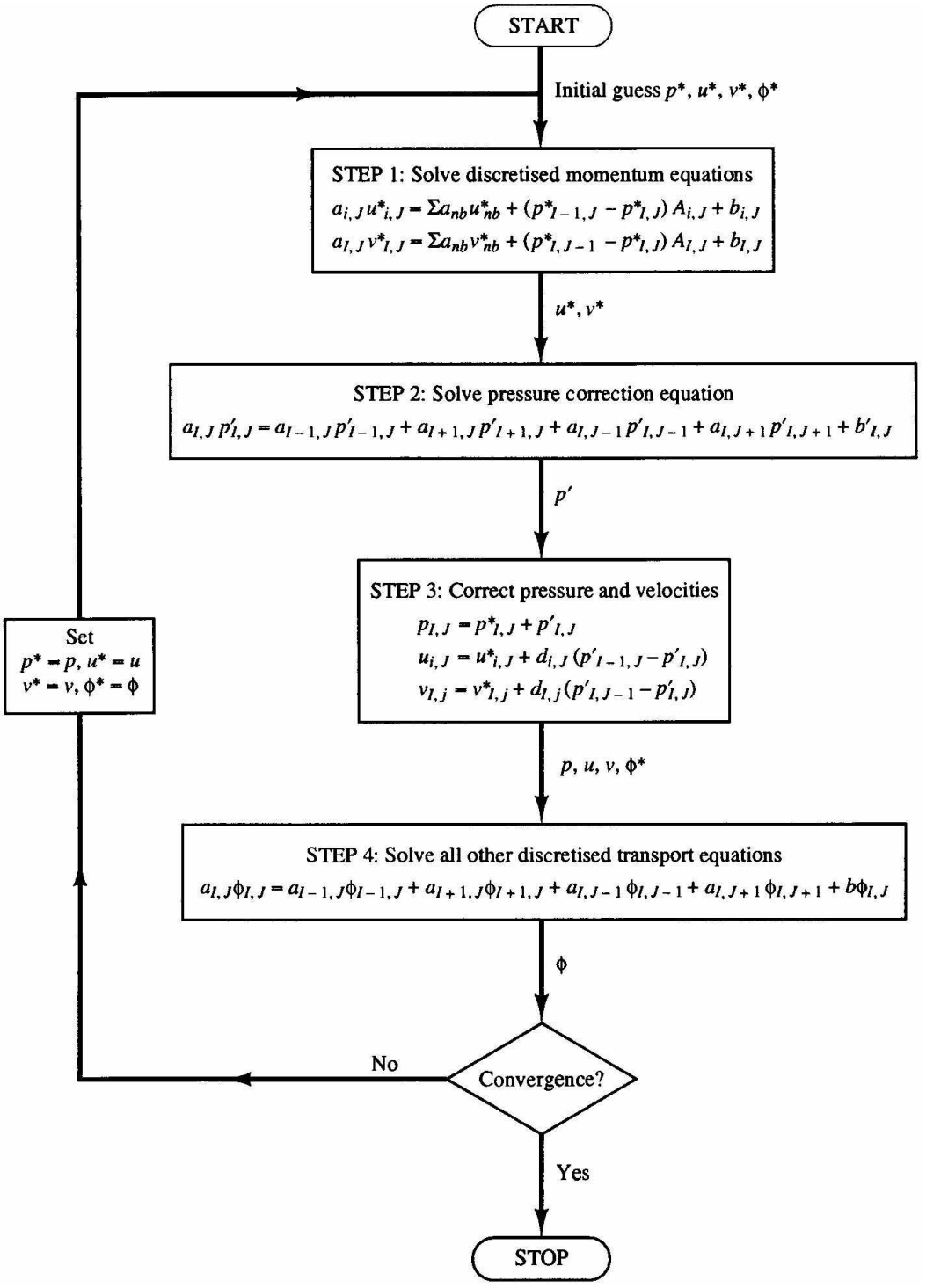

Figure 3.3. The SIMPLE Algorithm[16]

3.3.2. Scalar transport equations

3.3.2.1. Energy Equation. The energy equation is rearranged in terms of static temperature by excluding viscous dissipation and pressure work terms. Finally, the equation is written in the form of equation 3.21.

$$div\left(\rho \mathbf{u} T\right) = div\left(\frac{k}{c_p} grad T\right) - \sum \dot{\omega} \Delta h^0_{f,i} \tag{3.21}$$

The discretised form of the energy equation is given below. The coefficients are calculated by using hybrid scheme which is explained in section 3.2.1.

$$\begin{aligned} a_P T_P &= a_W T_W + a_E T_E + a_S T_S + a_N T_N + S_T \qquad (3.22) \\ \text{where} & \\ S_T &= -\dot{\omega} \Delta h_{combustion} \end{aligned}$$

3.3.2.2. Species mass continuity equation. The species mass continuity equation is written in the form of mass fractions of single species. It is to be solved for each species except nitrogen which is the inert portion of the reactant mixture for the problem.

$$div\left(\rho \mathbf{u} Y_i\right) = div\left(D_{i,m} grad Y_i\right) - \dot{\omega}_i \tag{3.23}$$

The discretised form of the equation is given below. The coefficients of discreti-

sation are calculated by hybrid scheme.

$$a_P Y_{i_P} = a_W Y_{i_W} + a_E Y_{i_E} + a_S Y_{i_S} + a_N Y_{i_N} + S_{Y_i} \tag{3.24}$$

where

$$S_{Y_i} = \dot{\omega}_i$$

3.4. Computational Grid

The computational grid consists of 140 by 140 grid points on the horizontal and vertical directions respectively. The spacing between grid points for this configuration is 0.0005 m. Nevertheless, there were some other grid configurations which were used in order to check the grid independency of the solver. The solution of continuity and momentum equations are checked for two other grids with the spacing of 0.00025 m (280 by 280 grid points) and 0.00016 m (420 by 420 grid points) and the current one is selected for the rest of the calculations. The Solution data is extracted along the midline on the first edge of the first roll and compared. The extracted horizontal velocity and the pressure data is plotted in figure 3.4.

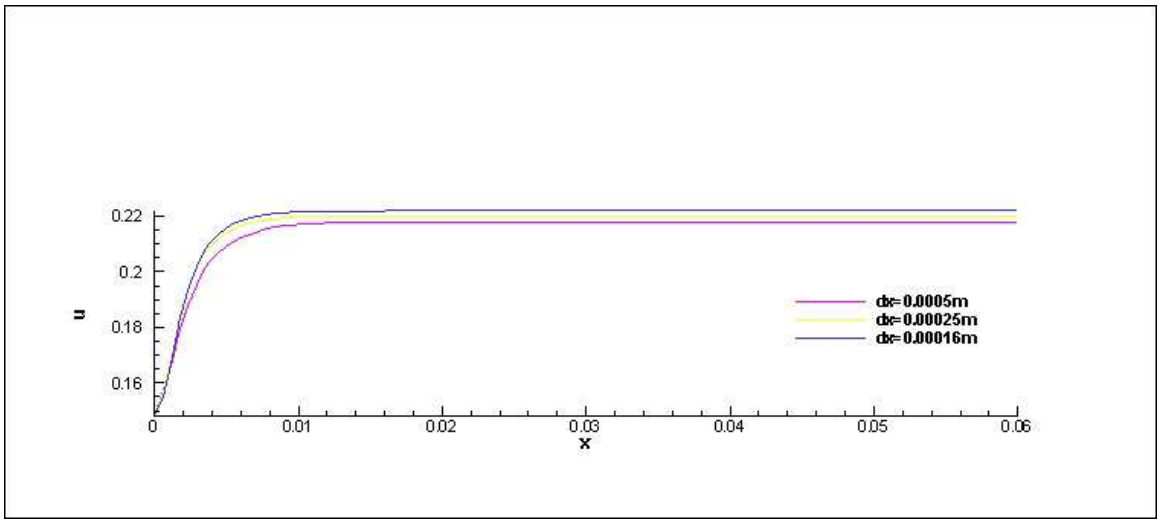

(a)

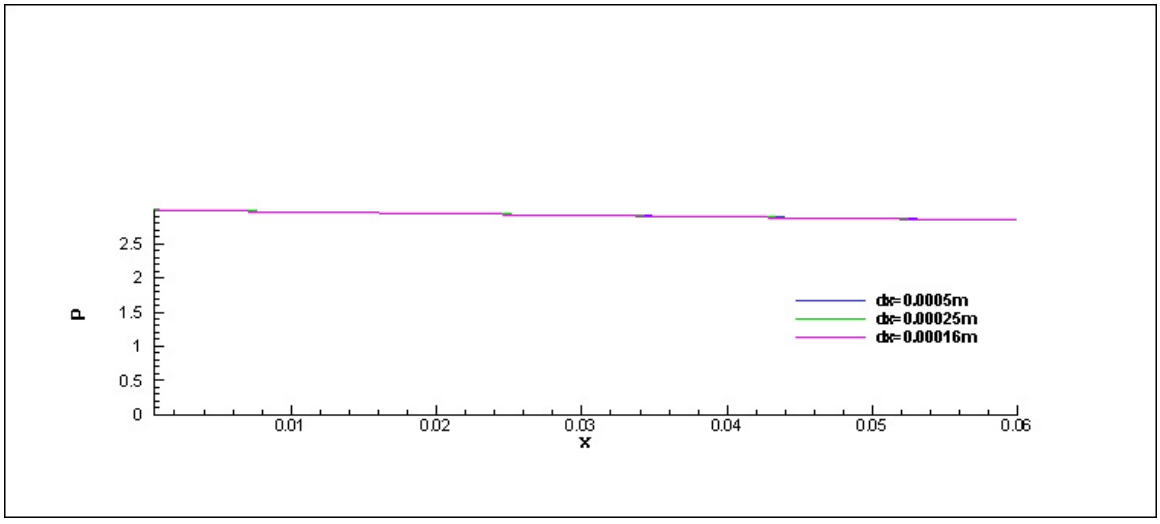

(b)

Figure 3.4. Grid independency check (a)Horizontal velocity along channel midline for three different spacing (b) Pressure along channel midline for three different spacing

3.5. Convergence Criterion

The flow equations and the other transport equations are calculated up to a certain point where the solution converges to the real solution of the equation sets. At that point the calculation is stopped and the solution is post processed. The level of convergence is calculated for x and y momentum equations and the other transport equations according to equation 3.25. The convergence of the pressure correction equation is checked by looking at the sum of the net mass flux of the computational control volumes. This value is non-dimensionalized by the maximum of the first five value.

$$R^{\phi} = \frac{\sum_{cellsP} |\sum_{nb} a_{nb}\phi_{nb} + b - a_p\phi_p|}{\sum_{cellsP} |a_p\phi_p|} \tag{3.25}$$

$$R^{c} = \sum_{cellsP} |rateofmasscreationincellP| \tag{3.26}$$

4. RESULTS AND DISCUSSIONS

The simulations of the Swiss roll type heat recirculation combustor are made for a range of Reynolds number and equivalence ratios, in order to investigate the characteristic of the combustor. In the simulations, inlet Re number varies from the value of 40 to 500. The inlet Re number and the equivalence ratio are computed as in equations 4.1 and 4.2 respectively.

$$Re = \frac{\rho U d}{\mu} \tag{4.1}$$

$$\phi = \frac{(F/A)_{inlet}}{(F/A)_{stoichiometric}} \tag{4.2}$$

where

U: Inlet velocity

d: channel height

$(F/A)_{inlet}$: Fuel air ratio at the inlet

$(F/A)_{stoichiometric}$: Stoichiometric fuel air ratio

4.1. Solver validation

The results of the solver is compared with the result obtained in [20]. A fairly good agreement is reached by comparing the temperature distribution. The distribution of temperature in the domain shown in figures 4.8(b) and 4.3(b) is not exactly match with the one of literature in figures 4.8(a) and 4.3(a)but the peak temperatures and the location of the peak temperature is close. On the other hand, the location of reaction zones shown in figures 4.2 and 4.4 are very similar. The differences might be due to the differences in solver parameters. The results obtained in the literature includes the heat loss in 3rd dimension and wall to wall radiation.

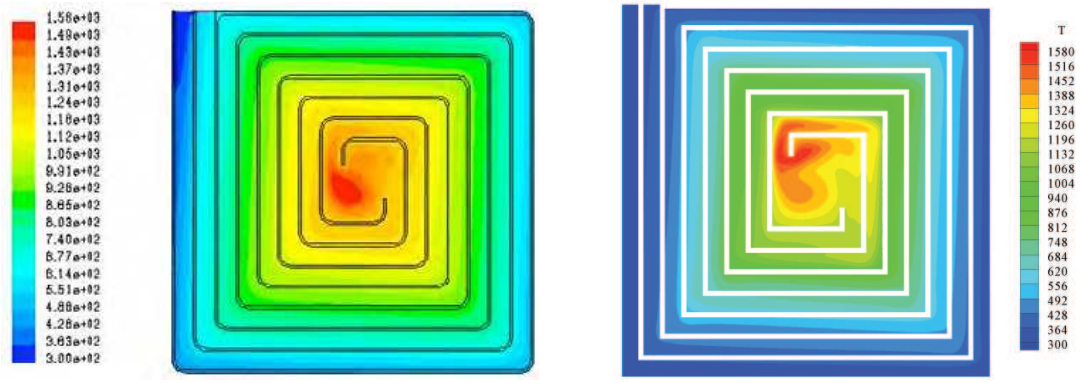

(a) (b)

Figure 4.1. The temperature distribution comparison for Re=40 (a) Results of Kuo [20] (b) Results of the solver

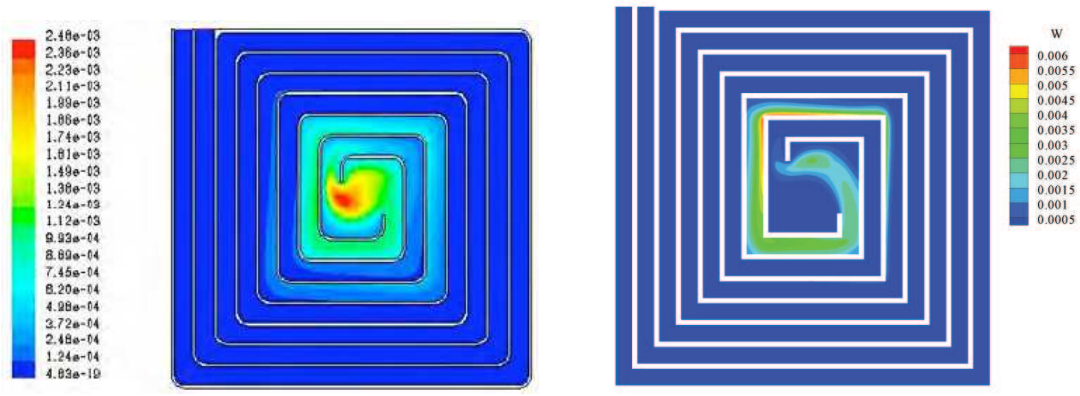

(a) (b)

Figure 4.2. The reaction rate distribution comparison for Re=40 (a) Results of Kuo [20] (b) Results of the solver

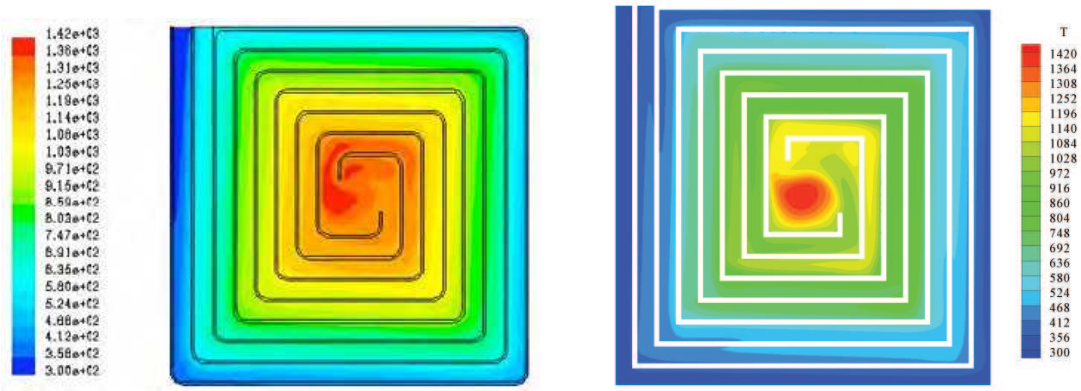

(a) (b)

Figure 4.3. The temperature distribution comparison for Re=100 (a) Results of Kuo [20] (b) Results of the solver

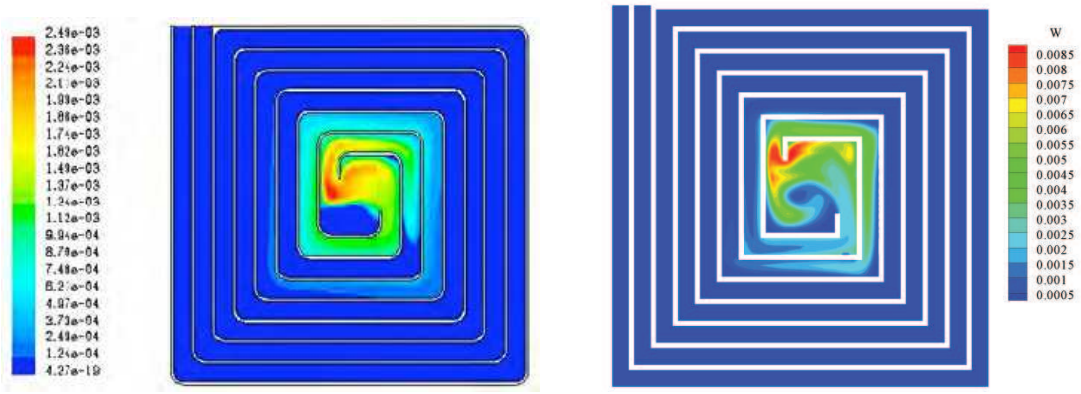

(a) (b)

Figure 4.4. The reaction rate distribution comparison for Re=100 (a) Results of Kuo [20] (b) Results of the solver

The drifts seen in the reaction rate terms is due to the fact that the solvers are using different pre-exponential factors in their reaction rate calculations. The one of Kuo [20] includes the wall to wall radiation and the heat loss in the third dimension.

4.2. Flow Inside The Combustor

The two dimensional flow field in the Swiss-roll combustor is determined in the whole domain considering the solid walls at the same time. The value of the constant source term in the momentum equations are set to be equal to a big number (10^100) so that the effect of the other term in the equation get much lower and therefore, the solution of the momentum equation on that grid point gets much closer to zero. Furthermore, this method is used to fix a value to a constant in a point.

The results for the pressure field inside combustor is obtained by setting the absolute pressure to zero at the exit of the combustor.

The velocity vectors and the streamlines for Re=40, 50, 100, and 500 cases are plotted from 4.5 to 4.8. On the left side of figures, the full scale plot of the combustor is given. On the right side, the magnified view of inner 2.5 roll part of the combustor is shown.

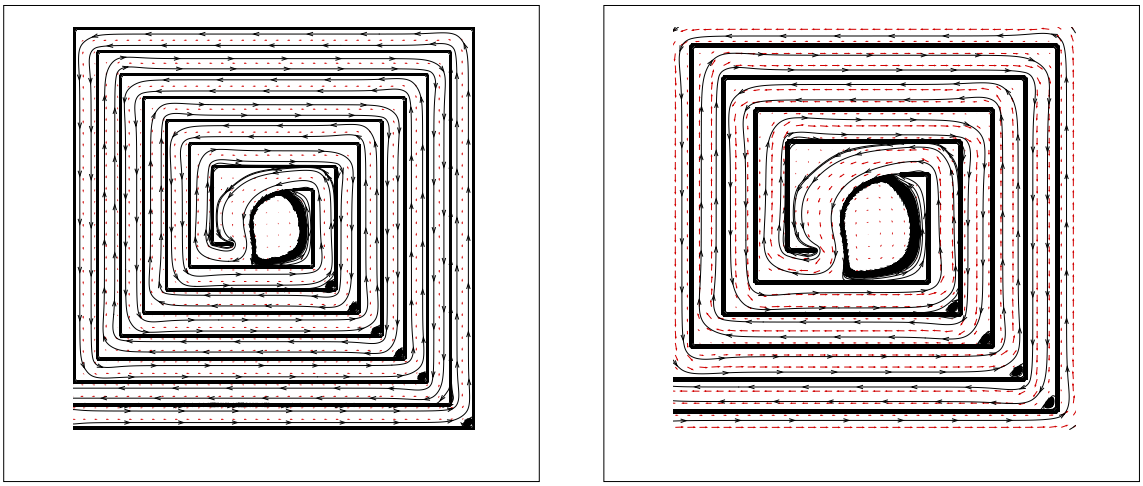

(a) (b)

Figure 4.5. Velocity vectors and streamlines of Swiss-roll reactor for Re=40 (a) Full view (b) Magnified view

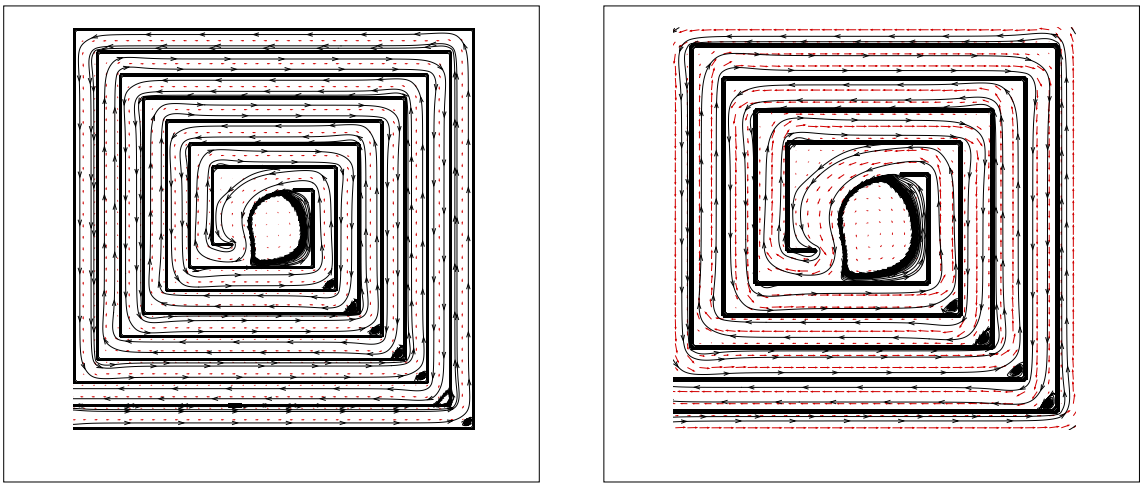

(a) (b)

Figure 4.6. Velocity vectors and streamlines of Swiss-roll reactor for Re=50 (a) Full view (b) Magnified view

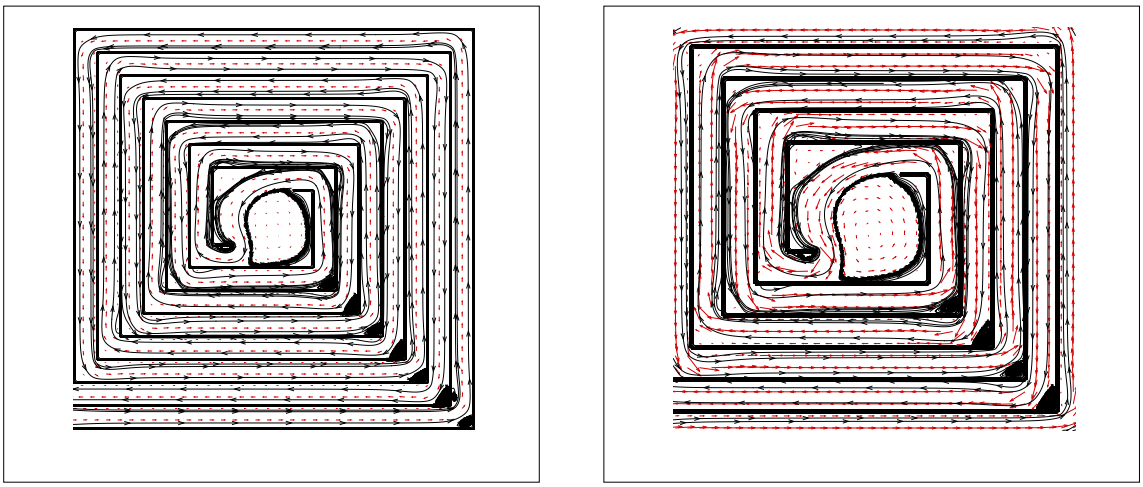

(a) (b)

Figure 4.7. Velocity vectors and streamlines of Swiss-roll reactor for Re=100 (a) Full view (b) Magnified view

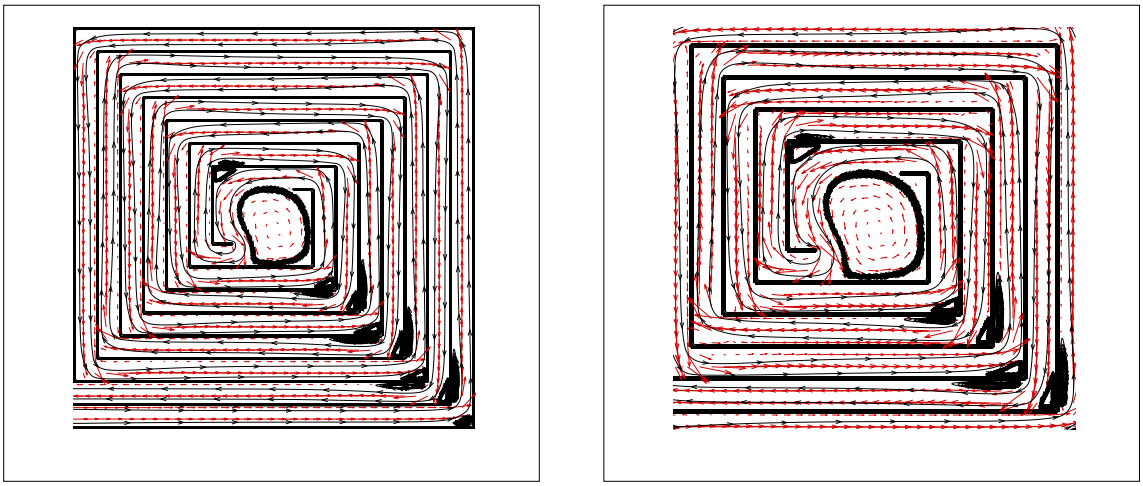

(a) (b)

Figure 4.8. Velocity vectors and streamlines of Swiss-roll reactor for Re=500 (a) Full view (b) Magnified view

As it is observed from figures, there are recirculation regions at the center and at all of the corners of the turning of the combustor. The recirculation regions at the corners are only shown on the lower right corners for representation purposes. They are observed on all of the corners. The flow cannot follow the wall boundaries. Main stream separates form the wall and some dead water regions are formed at sharp turnings. The low momentum fluid recirculates at the center region whereas the high momentum fluid is traveling around this area and continues its way to exit. The area of recirculating regions increases as the inlet Re of the flow increases. Convective heat transfer is very high on those areas. So, heat accumulates especially the one at the center. Therefore, it is the region with highest temperature.

4.3. Temperature and Species Distribution

The temperature, species distribution for the case Re=100 and $\phi = 0.43$ is given as an example in figures 4.9 and 4.11 respectively. It is observed in figure 4.10 that the reaction occurs at the center of the combustor. The peak temperature is almost located at the same place also. The species concentrations start to change at the path where the reaction mildly starts. It is noticeable in figures 4.11(c) and 4.11(d) that the products are accumulated in center and than dilutes to the main exit stream. This

may be due to the recirculation region observed in figure 4.7. The reaction zone is close to the recirculation zone. Therefore, reforming products are convectively transported to the dead air zone and due to the recirculating motion of the fluid they can not uniformly mixed with the main stream.

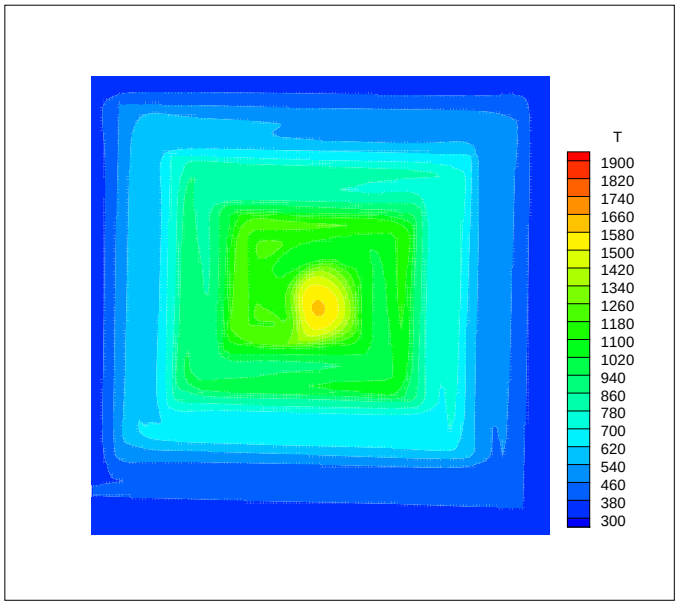

Figure 4.9. The temperature distribution in K (Re=100 and $\phi = 0.43$)

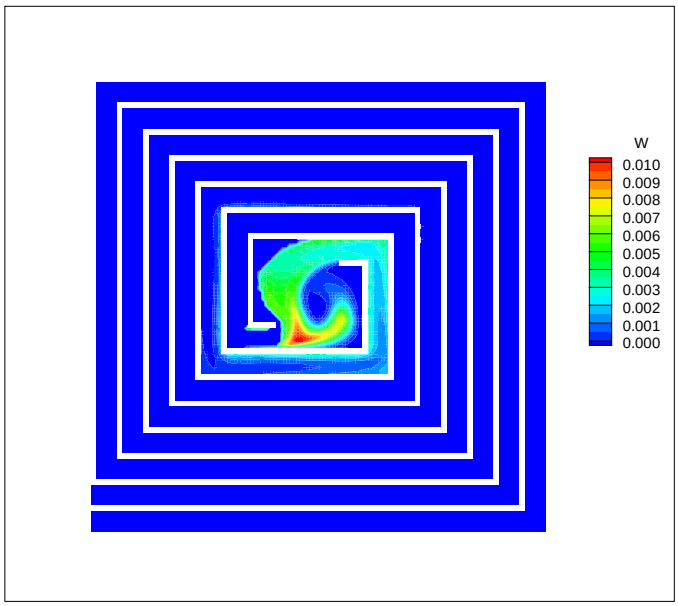

Figure 4.10. Reaction rate distribution in $(kmol/m^3 - s)$ (Re=100 and $\phi = 0.43$)

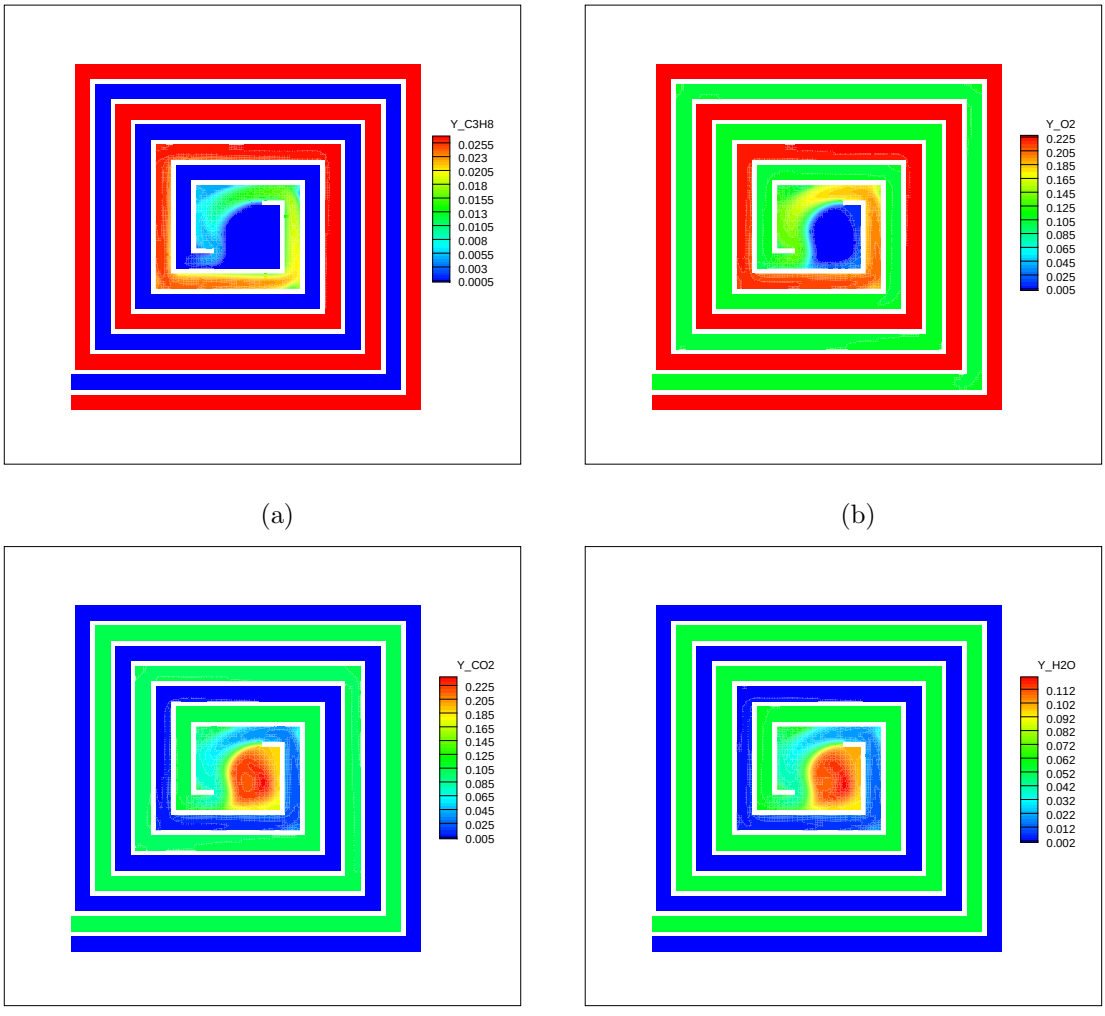

(a) (b)

(c) (d)

Figure 4.11. Mass fraction distributions of products and reactants in $(kmol/m^3 - s)$ (a)Propane, (b)Oxygen, (c)Carbon dioxide and (d)Water (Re=100 and$\phi = 0.43$)

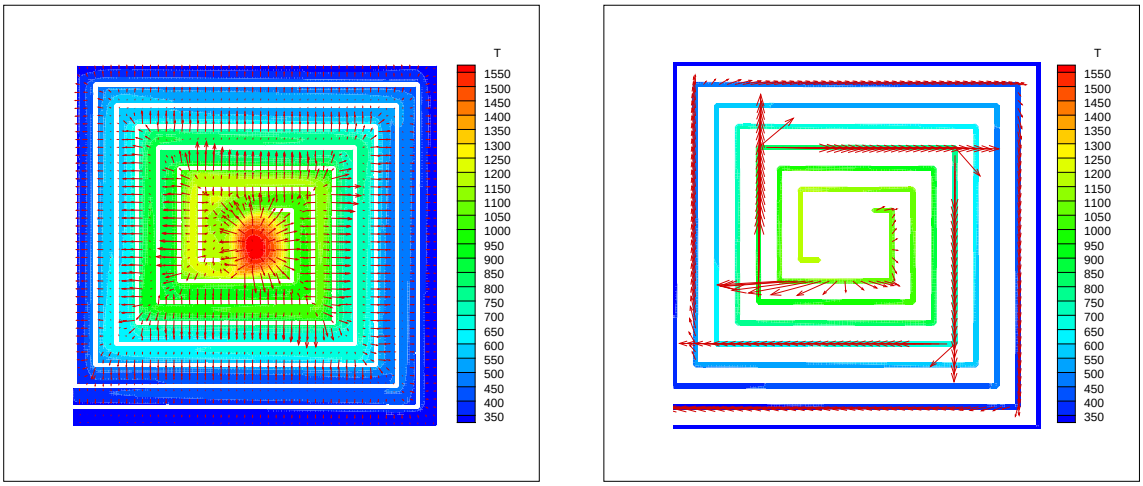

(a) (b)

Figure 4.12. Heat flux vectors on the temperature distribution(Re=100 and $\phi = 0.43$) (a) On the gas domain (b) On the solid domain

The heat flux vectors on top of temperature distribution are plotted in figure 4.12. The results show us that the maximum heat transfer is at the center of the combustor. As moving to the outer periphery, the amount of heat transfer decreases relatively. The dominant direction of heat transfer is always perpendicular to the streamwise direction and towards to the outer walls.

The heat transfer on the solid walls is directed from the central sections of the wall to the streamwise exit direction. The amount of heat transfer in the solid domain is relatively higher than the one in the fluid due to the very high thermal conductivity of the solid. On the other hand, the amount of heat transfer is much more greater in the middle region of the combustor than the periphery like in the gas domain.

4.4. Effect of Reynolds Number

The Reynolds number parameter is directly related to the velocity of the fluid. In other words, the convective characteristic of the flow is proportional to the Reynolds number. For the Swiss-roll combustor, as Re number increases for the reactant stream of the same equivalence ratio, the maximum temperature inside the domain increases. On the other hand, the reaction zone is pulled back to the inlet as Re increases. The investigation is done for the incoming mixture with equivalence ratio of 0.58 and the

Re number of 50, 60 and 70. The temperatures and reaction rates are plotted in 4.13, 4.14 and 4.15. The same fashion in magnification is applied on figures as applied on 4.5.

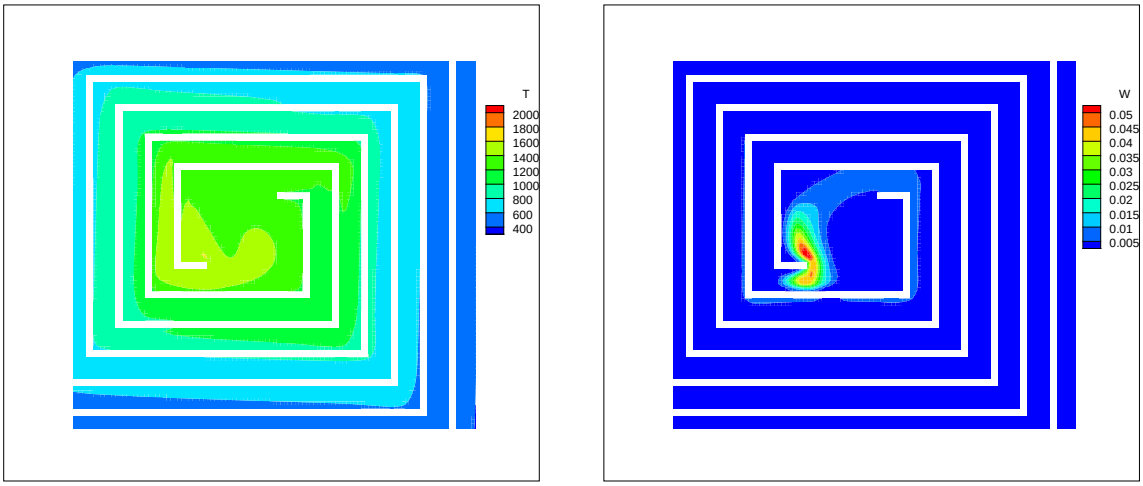

(a) (b)

Figure 4.13. The temperature and reaction rate distribution for Re=50 and $\phi = 0.58$ (a) Temperature Contours (b) Reaction rate contours

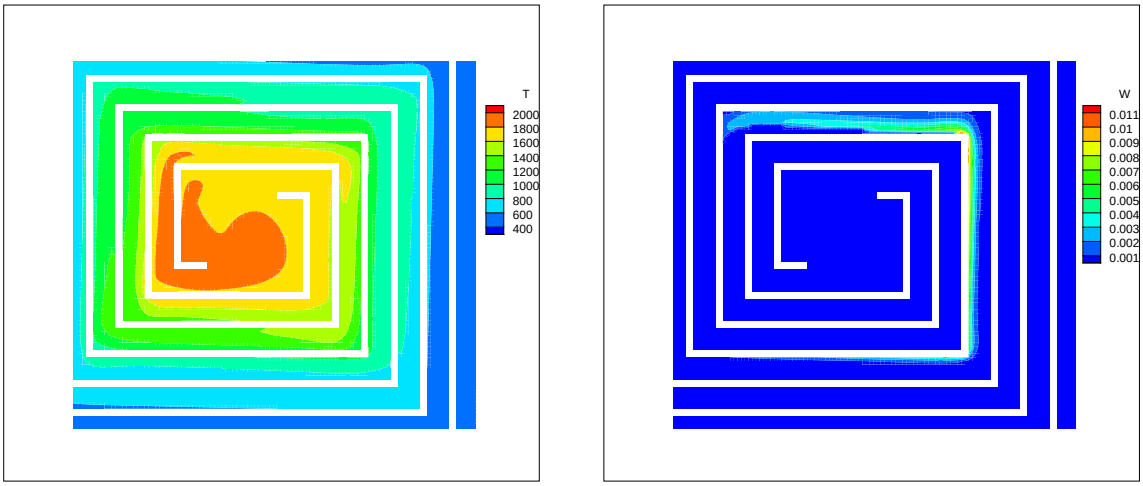

(a) (b)

Figure 4.14. The temperature and reaction rate distribution for Re=60 and $\phi = 0.58$ (a) Temperature Contours (b) Reaction rate contours

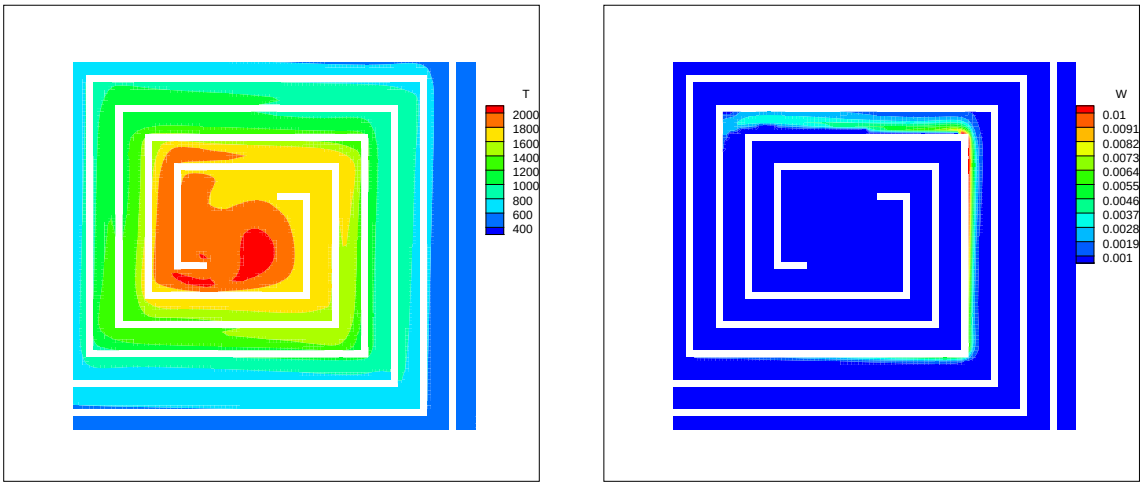

(a) (b)

Figure 4.15. The temperature and reaction rate distribution for Re=70 and $\phi = 0.58$ (a) Temperature Contours (b) Reaction rate contours

4.5. Effect of Equivalence Ratio

The equivalence ratio is another parameter to be investigated as a factor for combustion in a Swiss-roll. In order to understand the changes in the combustor due to changing equivalence ratio, the inlet Re is kept the same as 100 and the equivalence ratio of the incoming reactant stream is set to the values of 0.43, 0.45, 0.47, 0.51 for four different case. Those are the cases which are also investigated by Chen and Buckmaster [7].

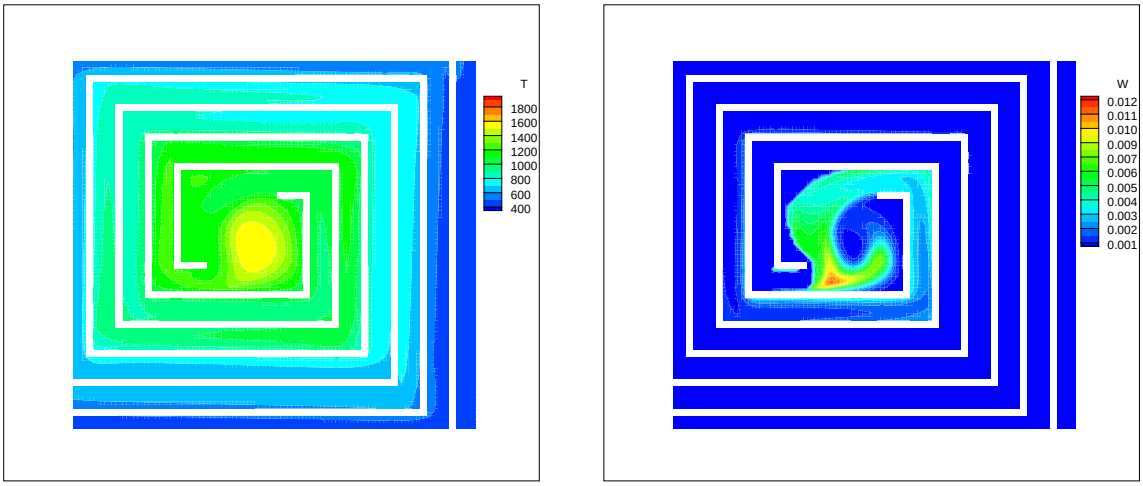

(a) (b)

Figure 4.16. The temperature and reaction rate distribution for Re=100 and $\phi = 0.43$ (a) Temperature distribution (K) (b) Reaction rate distribution ($kmol/m^3 - s$)

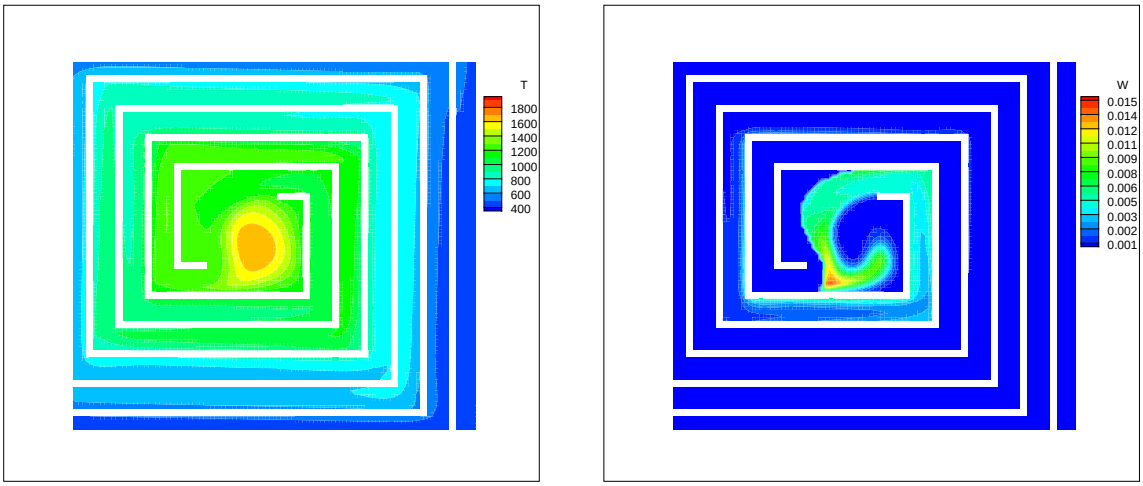

(a) (b)

Figure 4.17. The temperature and reaction rate distribution for Re=100 and $\phi = 0.45$ (a) Temperature distribution (K) (b) Reaction rate distribution ($kmol/m^3 - s$)

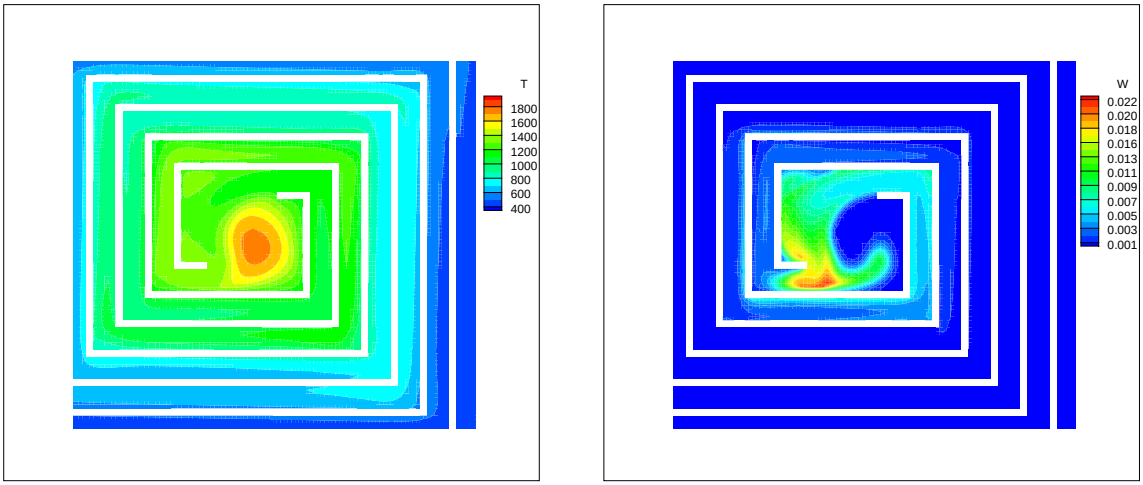

(a) (b)

Figure 4.18. The temperature and reaction rate distribution for Re=100 and $\phi = 0.47$ (a) Temperature distribution (K) (b) Reaction rate distribution ($kmol/m^3 - s$)

The effects of increasing ϕ are an increase in the maximum gas temperature and an increase in heat recirculation in the domain. The temperature of gas entering the combustion chamber increases with equivalence ratio. On the other hand, the location of maximum reaction and the maximum temperature does not change significantly for this Re number. Whereas, the starting point of the reaction is pulled back to the inlet by increasing the equivalence ratio.

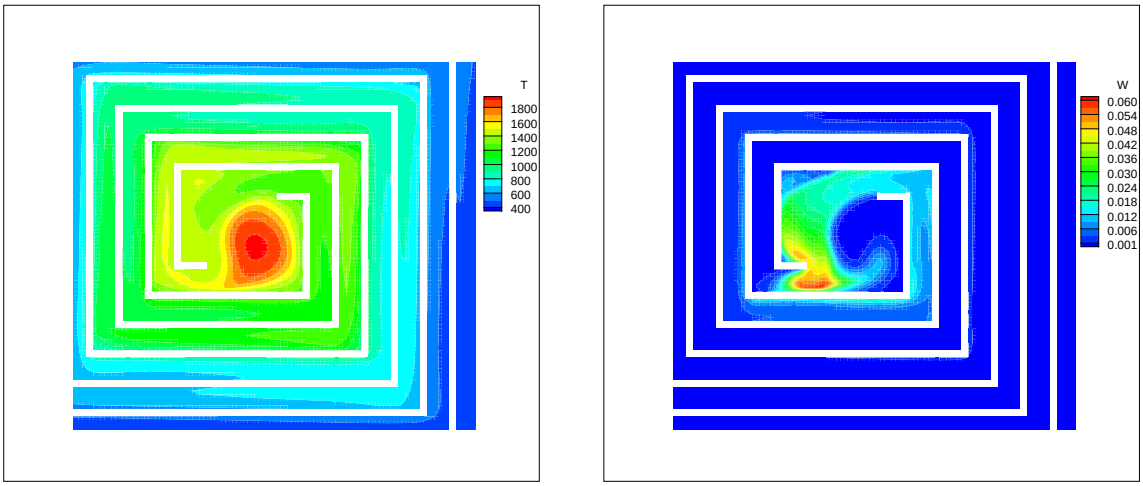

(a) (b)

Figure 4.19. The temperature and reaction rate distribution for Re=100 and $\phi = 0.51$ (a) Temperature distribution (K) (b) Reaction rate distribution ($kmol/m^3 - s$)

4.6. Effect of wall thermal conductivity

The wall thermal conductivity is an important parameter on heat recirculation in Swiss-roll combustor. The effect of wall thermal conductivity is shown in the 4.20. The investigation is done for Re=100 and Re=300 at the inlet of the flow field. All the solver parameters are kept the same except the wall thermal conductivity. The behavior of the extinction limit is such that as the conductivity decreases, the equivalence ratio at the extinction limit decreases as well. The heat transfer from the combustion zone to the walls decreases with decreasing thermal conductivity. Hence the fuel needed to sustain the flame is getting lower. This implies that the flame can be obtained for very low equivalence ratio in a Swiss-roll combustion chamber made of very poor conducting material.

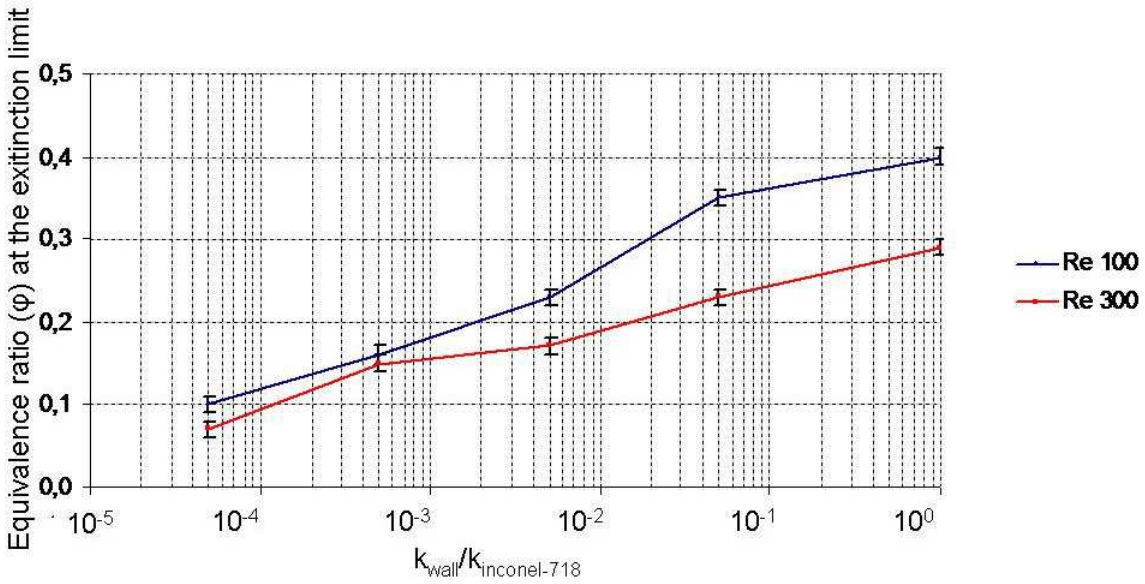

Figure 4.20. The effect of wall thermal conductivity on the extinction limit

5. CONCLUSIONS AND RECOMMENDATIONS

5.1. Conclusions

A meso-scale, rectangular, 3.5 turn Swiss-roll type, counter flow, heat - recirculating combustor is modeled with single step reaction mechanism. The effect of Reynolds number and the equivalence ratio is investigated.

The two dimensional momentum, energy and four species equations are solved simultaneously. The ideal gas equation is used as the state equation. The flow is assumed to be steady and laminar. So, a certain range of inlet Reynolds numbers are taken into consideration. The viscosity for fluid, conductivity and specific heats for the solid and the fluid is assumed to be constant and equal to a single value for the mixture. Whereas the binary diffusion coefficient of each species to the mixture is taken as a function of mixture composition and the values at 350 K are used for the binary diffusion coefficient for the couples of species on entire range of temperature. The gravity, pressure heating, radiation, viscous dissipation and Soret and Duffor effects are neglected in the energy equation.

The finite-volume approach is chosen to model the problem. An implicit, hybrid discretisation scheme which is second order accurate is used for space discretisation. The SIMPLE algorithm is employed in solution of momentum and continuity equations. The computational domain consists of both solid and fluid regions. Therefore, all of the equations are solved for both phases.

The result of the solver is compared with the results in the literature [20]. Due to the inclusion of heat loss in third dimension and wall to wall radiation, some differences observed but a fairly good agrement is reached in the sense that the peak temperature in the combustor.

The flow field is calculated for a wide range of Re number in the laminar range.

The recirculation zones are identified at the center and at the sharp corners of the combustor. The increasing Re has a positive effect on the area of recirculation zones. The recirculation zone causes product accumulation when the reaction is placed at the center of the combustor. On the other hand, as the Re increased in the laminar range for a fixed equivalence ratio, the reaction zone is observed to be pulled back to the inlet and the peak gas temperature increases. For the MEMS applications, the size of the combustor should be smaller. This implies reduction in the channel height and therefore inlet Re decreases. So it is likely to observe the reaction zone at the center of the combustor as the size of the combustor reduces.

The effect of equivalence ratio of incoming reactant stream is investigated by changing it at a fixed Re. It is observed that peak temperatures and reaction rates are increasing with increasing equivalence ratio. Moreover, the starting point of the combustion reaction is pulled back to the inlet.

The effect of the wall thermal conductivity on the extinction limits is investigated for the a fixed Reynolds number. It is observed that lean extinction limit equivalence ratio significantly reduces with reducing temperature because the heat transfer from the reaction zone to the walls are reduced.

5.2. Future Work

The present solver neglects three dimensional effect whereas the heat loss in the third dimension can be added to get closer to the reality. Furthermore, the surface/gas radiation heat transfer can be added as a mode of heat transfer. A turbulence model can be employed to be able to simulate high inlet velocity therefore high mass flow rate cases. The detailed chemistry can be used for more realistic chemical modeling. The effect of catalytic surfaces on the peak temperatures and the extinction limits can be analyzed. More accurate discretisation schemes can be tried in order to higher the accuracy of the solver. The material properties are assumed to be constant. However they are changing considerably within the operating range of the combustor. So the material properties can be taken as functions of temperature. Moreover, different kind

of fuels and different kind of solid structures can be modeled to understand better the combustor.

APPENDIX A: SIMPLIFICATIONS OF THE FLOW EQUATIONS WITH NON-DIMENSIONAL ANALYSIS

A.1. Continuity Equation

This section is to derive the first governing equation which is *the continuity equation*:

$$\frac{\partial \rho}{\partial t} + div \cdot (\rho \overrightarrow{V}) = 0 \qquad \text{(General Form)[21]} \tag{A.1}$$

$$\frac{\cancel{\partial \rho}}{\cancel{\partial t}}^{=0\ \text{Steady–State}} + \frac{\partial(\rho u)}{\partial x} + \frac{\partial(\rho v)}{\partial y} + \cancel{\frac{\partial(\rho w)}{\partial z}}^{=0\ \text{2–D}} = 0$$

$$\frac{\partial(\rho u)}{\partial x} + \frac{\partial(\rho v)}{\partial y} = 0 \qquad \text{(Final Form)} \tag{A.2}$$

A.2. Momentum Equations

This section is to derive the momentum equations for well-known Navier–Stokes equations. The general form of the equation is given below.[21]

A.3. *x*–Component

$$\frac{\rho}{g_c}\frac{Du}{Dt} = B_x - \frac{\partial p}{\partial x} + \frac{\partial}{\partial x}[\mu(2\frac{\partial u}{\partial x} - \frac{2}{3} div \cdot \overrightarrow{V})] + \frac{\partial}{\partial y}[\mu(\frac{\partial u}{\partial y} + \frac{\partial v}{\partial x})] + \cancel{\frac{\partial}{\partial z}[\mu(\frac{\partial w}{\partial x} + \frac{\partial u}{\partial z})]} \tag{A.3}$$

where

g_c : dimensionalization constant $= 1\,kg\ m/N\ s^2$ in SI and $= 32.2\,lb_m\ ft/lb_f\ sec^2$ in English units

B_x : body force which is zero in this case

μ : dynamic viscosity

$\overrightarrow{V}$: 2–D velocity vector which is $\overrightarrow{V} = u\,\overrightarrow{i} + v\,\overrightarrow{j}$

p : pressure

The simplified, explicit, and conservative form of the equation is:

$$\frac{1}{g_c}\left(\frac{\partial(\rho uu)}{\partial x} + \frac{\partial(\rho uv)}{\partial y}\right) = -\frac{\partial p}{\partial x} + \frac{2}{3}\frac{\partial \mu}{\partial x}\left(2\frac{\partial u}{\partial x} - \frac{\partial v}{\partial y}\right) + \mu\left(\frac{4}{3}\frac{\partial^2 u}{\partial x^2} + \frac{\partial^2 u}{\partial y^2} + \frac{1}{3}\frac{\partial^2 v}{\partial x \partial y}\right) + \frac{\partial \mu}{\partial y}\left(\frac{\partial u}{\partial y} + \frac{\partial v}{\partial x}\right) \tag{A.4}$$

A.4. *y*–Component

$$\frac{\rho}{g_c}\frac{Dv}{Dt} = B_y - \frac{\partial p}{\partial y} + \frac{\partial}{\partial x}[\mu(\frac{\partial u}{\partial y} + \frac{\partial v}{\partial x})] + \frac{\partial}{\partial y}[\mu(2\frac{\partial v}{\partial y} - \frac{2}{3} div \cdot \overrightarrow{V})] + \cancel{\frac{\partial}{\partial z}[\mu(\frac{\partial v}{\partial z} + \frac{\partial w}{\partial y})]} \tag{A.5}$$

The most simplified, explicit, and conservative form of the equation is:

$$\frac{1}{g_c}\left(\frac{\partial(\rho uv)}{\partial x} + \frac{\partial(\rho vv)}{\partial y}\right) = -\frac{\partial p}{\partial y} + \frac{2}{3}\frac{\partial \mu}{\partial y}\left(2\frac{\partial v}{\partial y} - \frac{\partial u}{\partial x}\right) + \mu\left(\frac{4}{3}\frac{\partial^2 v}{\partial y^2} + \frac{\partial^2 v}{\partial x^2} + \frac{1}{3}\frac{\partial^2 u}{\partial y \partial x}\right) + \frac{\partial \mu}{\partial x}\left(\frac{\partial u}{\partial y} + \frac{\partial v}{\partial x}\right) \tag{A.6}$$

A.5. Non-Dimensionalization of Momentum Equations

The non-dimensional parameter are listed below:

$$x^* = \frac{x}{l} \qquad y^* = \frac{y}{l} \qquad u^* = \frac{u}{v} \qquad v^* = \frac{v}{\mathrm{v}} \qquad p^* = \frac{p}{p_0} \qquad \rho^* = \frac{\rho}{\rho_0} \qquad \mu^* = \frac{\mu}{\mu_0}$$

$$\frac{\partial}{\partial x} = \frac{1}{l}\frac{\partial}{\partial x^*} \quad \frac{\partial}{\partial y} = \frac{1}{l}\frac{\partial}{\partial y^*} \quad \frac{\partial^2}{\partial x^2} = \frac{1}{l^2}\frac{\partial^2}{\partial x^{*2}} \quad \frac{\partial^2}{\partial y^2} = \frac{1}{l^2}\frac{\partial^2}{\partial y^{*2}} \quad \frac{\partial^2}{\partial x \partial y} = \frac{1}{l^2}\frac{\partial^2}{\partial x^* \partial y^*}$$

$$\begin{aligned}\frac{\rho_0 \mathrm{v}^2}{l}\Big[\frac{\partial(\rho^* u^* u^*)}{\partial x^*} + \frac{\partial(\rho^* u^* v^*)}{\partial y^*}\Big] = -\frac{p_0}{l}\frac{\partial p^*}{\partial x^*} + \frac{2}{3}\frac{\mu_0 \mathrm{v}}{l^2}\frac{\partial \mu^*}{\partial x^*}\Big(2\frac{\partial u^*}{\partial x^*} - \frac{\partial v^*}{\partial y^*}\Big) + \\ \Big[\frac{\mu_0 \mathrm{v}}{l^2}\Big]\mu^*\Big(\frac{4}{3}\frac{\partial^2 u^*}{\partial x^{*2}} + \frac{\partial^2 u^*}{\partial y^{*2}} + \frac{1}{3}\frac{\partial^2 v^*}{\partial x^* \partial y^*}\Big) + \Big[\frac{\mu_0 \mathrm{v}}{l^2}\Big]\frac{\partial \mu^*}{\partial y^*}\Big[\frac{\partial u^*}{\partial y^*} + \frac{\partial v^*}{\partial x^*}\Big] \qquad \text{(A.7)}\end{aligned}$$

$$\begin{aligned}\frac{\rho_0 \mathrm{v}^2}{l}\Big[\frac{\partial(\rho^* u^* u^*)}{\partial x^*} + \frac{\partial(\rho^* u^* v^*)}{\partial y^*}\Big] = -\frac{p_0}{l}\frac{\partial p^*}{\partial x^*} + \frac{\mu_0 \mathrm{v}}{l^2}\Bigg\{\frac{2}{3}\frac{\partial \mu^*}{\partial x^*}\Big(2\frac{\partial u^*}{\partial x^*} - \frac{\partial v^*}{\partial y^*}\Big) + \\ \mu^*\Big(\frac{4}{3}\frac{\partial^2 u^*}{\partial x^{*2}} + \frac{\partial^2 u^*}{\partial y^{*2}} + \frac{1}{3}\frac{\partial^2 v^*}{\partial x^* \partial y^*}\Big) + \frac{\partial \mu^*}{\partial y^*}\Big[\frac{\partial u^*}{\partial y^*} + \frac{\partial v^*}{\partial x^*}\Big]\Bigg\} \qquad \text{(A.8)}\end{aligned}$$

By multiplying each side with $\rho_0 \mathrm{v}^2/l$ we get non-dimensional x-momentum equation:

$$\begin{aligned}\Big[\frac{\partial(\rho^* u^* u^*)}{\partial x^*} + \frac{\partial(\rho^* u^* v^*)}{\partial y^*}\Big] &= -\frac{\overbrace{p_0}^{Eu}}{\rho_0 \mathrm{v}^2}\frac{\partial p^*}{\partial x^*} + \frac{\overbrace{\mu_o}^{1/Re}}{\rho_0 \mathrm{v} l}\Bigg\{\frac{2}{3}\frac{\partial \mu^*}{\partial x^*}\Big(2\frac{\partial u^*}{\partial x^*} - \frac{\partial v^*}{\partial y^*}\Big) + \mu^*\Big(\frac{4}{3}\frac{\partial^2 u^*}{\partial x^{*2}} \\ &\quad + \frac{\partial^2 u^*}{\partial y^{*2}} + \frac{1}{3}\frac{\partial^2 v^*}{\partial x^* \partial y^*}\Big) + \frac{\partial \mu^*}{\partial y^*}\Big[\frac{\partial u^*}{\partial y^*} + \frac{\partial v^*}{\partial x^*}\Big]\Bigg\} \qquad \text{(A.9)}\end{aligned}$$

The non-dimensional y-momentum equation is found in similar way:

$$\begin{aligned}\Big[\frac{\partial(\rho^* u^* v^*)}{\partial x^*} + \frac{\partial(\rho^* v^* v^*)}{\partial y^*}\Big] &= -Eu\frac{\partial p^*}{\partial y^*} + \frac{1}{Re}\Bigg\{\frac{2}{3}\frac{\partial \mu^*}{\partial y^*}\Big(2\frac{\partial v^*}{\partial y^*} - \frac{\partial u^*}{\partial x^*}\Big) + \mu^*\Big(\frac{4}{3}\frac{\partial^2 v^*}{\partial y^{*2}} + \\ &\quad \frac{\partial^2 v^*}{\partial x^{*2}} + \frac{1}{3}\frac{\partial^2 u^*}{\partial x^* \partial y^*}\Big) + \frac{\partial \mu^*}{\partial x^*}\Big[\frac{\partial u^*}{\partial y^*} + \frac{\partial v^*}{\partial x^*}\Big]\Bigg\} \qquad \text{(A.10)}\end{aligned}$$

A.6. The Source Term of The x-momentum Equation

$$\frac{\partial(\rho uu)}{\partial x}+\frac{\partial(\rho uv)}{\partial y}=-\frac{\partial p}{\partial x}+\frac{\partial}{\partial x}\left[\mu\left(2\frac{\partial u}{\partial x}-\frac{2}{3}div(\overrightarrow{V})\right)\right]+\frac{\partial}{\partial y}\left[\mu\left(\frac{\partial u}{\partial y}+\frac{\partial v}{\partial x}\right)\right] \quad \text{(A.11)}$$

If the above equation is tried to be resembled to which is in the main program[16]

$$\begin{aligned}\frac{\partial}{\partial x}(\rho uu)+\frac{\partial}{\partial y}(\rho uv)= \quad & -\frac{\partial p}{\partial x}+\frac{\partial}{\partial x}\left[\mu\left(\frac{\partial u}{\partial x}\right)\right]+\frac{\partial}{\partial x}\left[\mu\left(\frac{\partial u}{\partial x}\right)\right]+\frac{\partial}{\partial y}\left[\mu\left(\frac{\partial u}{\partial y}\right)\right] \\ & +\frac{\partial}{\partial y}\left[\mu\left(\frac{\partial v}{\partial x}\right)\right]-\frac{\partial}{\partial x}\left[\mu\left(\frac{2}{3}div(\overrightarrow{V}\right)\right] \end{aligned} \quad \text{(A.12)}$$

$$\begin{aligned}\underbrace{\frac{\partial}{\partial x}(\rho uu)+\frac{\partial}{\partial y}(\rho uv)}_{\text{Convective terms}}=\underbrace{\frac{\partial}{\partial x}\left[\mu\left(\frac{\partial u}{\partial x}\right)\right]+\frac{\partial}{\partial y}\left[\mu\left(\frac{\partial u}{\partial y}\right)\right]}_{\text{Diffusive terms}} \quad \underbrace{-\frac{\partial p}{\partial x}}_{\text{Pressure variation term}} \\ \underbrace{+\frac{\partial}{\partial x}\left[\mu\left(\frac{\partial u}{\partial x}\right)\right]+\frac{\partial}{\partial y}\left[\mu\left(\frac{\partial v}{\partial x}\right)\right]-\frac{\partial}{\partial x}\left[\mu\left(\frac{2}{3}div(\overrightarrow{V})\right)\right]}_{\text{The source term Su}} \end{aligned} \quad \text{(A.13)}$$

$$\begin{aligned}S_u&=\frac{\partial}{\partial x}\left(\mu\frac{\partial u}{\partial x}\right)+\frac{\partial}{\partial y}\left(\mu\frac{\partial v}{\partial x}\right)-\frac{\partial}{\partial x}\left[\mu\left(\frac{2}{3}\left(\frac{\partial u}{\partial x}+\frac{\partial v}{\partial y}\right)\right)\right] \\ S_u&=\frac{\partial}{\partial x}\left(\mu\frac{\partial u}{\partial x}\right)+\frac{\partial}{\partial y}\left(\mu\frac{\partial v}{\partial x}\right)-\frac{2}{3}\frac{\partial}{\partial x}\left(\mu\frac{\partial u}{\partial x}\right)-\frac{2}{3}\frac{\partial}{\partial x}\left(\mu\frac{\partial v}{\partial y}\right) \\ S_u&=\frac{1}{3}\frac{\partial}{\partial x}\left(\mu\frac{\partial u}{\partial x}\right)+\frac{\partial}{\partial y}\left(\mu\frac{\partial v}{\partial x}\right)-\frac{2}{3}\frac{\partial}{\partial x}\left(\mu\frac{\partial v}{\partial y}\right) \end{aligned} \quad \text{(A.14)}$$

A.7. The Source Term of the y-momentum Equation

$$\frac{\partial(\rho uv)}{\partial x}+\frac{\partial(\rho vv)}{\partial y}=-\frac{\partial p}{\partial y}+\frac{\partial}{\partial x}\left[\mu\left(\frac{\partial u}{\partial y}+\frac{\partial v}{\partial x}\right)\right]+\frac{\partial}{\partial y}\left[\mu\left(2\frac{\partial v}{\partial y}-\frac{2}{3}div(\overrightarrow{V})\right)\right] \quad \text{(A.15)}$$

If the above equation is tried to be resembled to which is in the main program[16]

$$\overbrace{\frac{\partial}{\partial x}(\rho uv)+\frac{\partial}{\partial y}(\rho vv)}^{\text{Convective terms}} = \overbrace{-\frac{\partial p}{\partial y}}^{\text{Pressure variation term}} \underbrace{+\overbrace{\frac{\partial}{\partial x}\left[\mu\left(\frac{\partial v}{\partial x}\right)\right]+\frac{\partial}{\partial y}\left[\mu\left(\frac{\partial v}{\partial y}\right)\right]}^{\text{Diffusive terms}} +\frac{\partial}{\partial x}\left[\mu\left(\frac{\partial u}{\partial y}\right)\right]+\frac{\partial}{\partial y}\left[\mu\left(\frac{\partial v}{\partial y}\right)\right]-\frac{2}{3}\frac{\partial}{\partial y}\left[\left(\mu\cdot div(\overrightarrow{V}\right)\right]}_{\text{The source term Sv}}$$

$$\begin{aligned} S_v &= \frac{\partial}{\partial x}\left(\mu\frac{\partial u}{\partial y}\right)+\frac{\partial}{\partial y}\left(\mu\frac{\partial v}{\partial y}\right)-\frac{2}{3}\frac{\partial}{\partial y}\left[\mu\left(\left(\frac{\partial u}{\partial x}+\frac{\partial v}{\partial y}\right)\right)\right] \\ &= \frac{\partial}{\partial x}\left(\mu\frac{\partial u}{\partial y}\right)+\frac{\partial}{\partial y}\left(\mu\frac{\partial v}{\partial y}\right)-\frac{2}{3}\frac{\partial}{\partial y}\left(\mu\frac{\partial u}{\partial x}\right)-\frac{2}{3}\frac{\partial}{\partial y}\left(\mu\frac{\partial v}{\partial y}\right) \\ S_v &= \frac{\partial}{\partial x}\left(\mu\frac{\partial u}{\partial y}\right)+\frac{1}{3}\frac{\partial}{\partial y}\left(\mu\frac{\partial v}{\partial y}\right)-\frac{2}{3}\frac{\partial}{\partial y}\left(\mu\frac{\partial u}{\partial x}\right) \end{aligned} \tag{A.16}$$

A.8. Species Mass Continuity Equation

Because the fluid is considered as multi–component fluid, the species mass continuity equations must be satisfied for each component of the fluid. [12]

$$\rho(\cancel{\frac{\partial Y_i}{\partial t}}+u\frac{\partial Y_i}{\partial x}+v\frac{\partial Y_i}{\partial y}+\cancel{w\frac{\partial Y_i}{\partial z}})+\frac{\partial}{\partial x}(\rho Y_i V_{ix})+\frac{\partial}{\partial y}(\rho Y_i V_{iy})+\cancel{\frac{\partial}{\partial z}(\rho Y_i V_{iz})} = \dot{\omega}_i[12] \tag{A.17}$$

($\cancel{\frac{\partial Y_i}{\partial t}}$: = 0 Steady–State; $\cancel{w\frac{\partial Y_i}{\partial z}}$: = 0 2–D; $\cancel{\frac{\partial}{\partial z}(\rho Y_i V_{iz})}$: = 0 2–D)

$$V_{ix}=-\frac{D}{Y_i}\frac{\partial Y_i}{\partial x} \qquad V_{iy}=-\frac{D}{Y_i}\frac{\partial Y_i}{\partial y} \qquad V_{iz}=-\frac{D}{Y_i}\frac{\partial Y_i}{\partial z}$$

where

$\dot{\omega}_i$:rate of mass production of the species i

D :Binary diffusivity

Y_i :Mass fraction of ith species which is $Y_i=\frac{\rho_i}{\rho}$

The simplified, explicit and conservative form of the equation set i

$$\frac{\partial(\rho u Y_i)}{\partial x} + \frac{\partial(\rho v Y_i)}{\partial y} = \frac{\partial}{\partial x}(\rho D \frac{\partial Y_i}{\partial x}) + \frac{\partial}{\partial y}(\rho D \frac{\partial Y_i}{\partial y}) + \dot{\omega}_i \tag{A.18}$$

A.9. Energy Equation

The energy equation is used to calculate the temperature of the mixture throughout the domain. The implicit form is given below. [21]

$$\begin{aligned} \rho c_p \frac{DT}{Dt} &= div \cdot (q'') + q''' + \beta T \frac{Dp}{Dt} + \mu\Phi \\ q'' &= -\lambda \overrightarrow{\nabla} T \end{aligned} \tag{A.19}$$

where c_p :specific heat

q'' :the rate of heat transfer

λ :thermal conductivity

q''' :the rate of heat generated

β :the coefficient of thermal expansion

Φ :viscous dissipation

$$\begin{aligned} \beta &= \frac{1}{\rho}(\frac{\partial \rho}{\partial T})_{p=constant} \\ \Phi &= 2[(\frac{\partial u}{\partial x})^2 + (\frac{\partial v}{\partial y})^2 + \cancelto{= 0\ 2\text{–D}}{(\frac{\partial w}{\partial z})^2}] - \frac{2}{3}[div(\overrightarrow{V}]^2) + (\frac{\partial u}{\partial y} + \frac{\partial v}{\partial x})^2 \\ &\quad + \cancel{(\frac{\partial v}{\partial z} + \frac{\partial w}{\partial y})^2} + \cancel{(\frac{\partial w}{\partial x} + (\frac{\partial u}{\partial z})^2} \end{aligned}$$

The simplified for of the viscous dissipation is:

$$\Phi = 2[(\frac{\partial u}{\partial x})^2 + (\frac{\partial v}{\partial y})^2] - \frac{2}{3}[div(\overrightarrow{V}]^2) + (\frac{\partial u}{\partial y} + \frac{\partial v}{\partial x})^2 \tag{A.20}$$

The most explicit and simplified form of the equation is:

$$\begin{aligned}\rho c_p(u\frac{\partial T}{\partial x}+v\frac{\partial T}{\partial y}) &= \frac{\partial k}{\partial x}\frac{\partial T}{\partial x}+k\frac{\partial^2 T}{\partial x^2}+\frac{\partial k}{\partial y}\frac{\partial T}{\partial y}+k\frac{\partial^2 T}{\partial y^2}+q'''+\beta T(u\frac{\partial p}{\partial x}+v\frac{\partial p}{\partial y})\\ &+\mu\{\frac{1}{3}[(\frac{\partial u}{\partial x})^2+(\frac{\partial v}{\partial y})^2]+(\frac{\partial u}{\partial y})^2+(\frac{\partial v}{\partial x})^2+2(\frac{\partial u}{\partial y}\frac{\partial v}{\partial x})\\ &-\frac{2}{3}(\frac{\partial u}{\partial x}\frac{\partial v}{\partial y})\} \qquad (A.21)\end{aligned}$$

A.10. Non-Dimensionalization of Energy Equation

The non-dimensional variables are the same as in momentum equations but some more is added to the system:

$$\begin{aligned}\theta &= \frac{T-T_r}{\Delta T} \qquad k=k^*k_0\\ \frac{c_p\rho_0 \mathrm{v}}{l\Delta T}(\frac{\partial(\rho^* u^*\theta)}{\partial x^*}+\frac{(\partial\rho^* v^*\theta)}{\partial y^*}) &= \frac{k_0}{l^2\Delta T}\left(\frac{\partial k^*}{\partial x^*}\frac{\partial\theta}{\partial x^*}+k^*\frac{\partial^2\theta}{\partial x^{*^2}}+\frac{\partial k^*}{\partial y^*}\frac{\partial\theta}{\partial y^*}+k\frac{\partial^2\theta}{\partial y^{*^2}}\right)\\ &+q'''+\beta(\theta+T_r)\frac{p_0\mathrm{v}\Delta T}{l}\left(u^*\frac{\partial p^*}{\partial x^*}+v^*\frac{\partial p^*}{\partial y^*}\right)\\ &+\frac{\mu_0\mathrm{v}^2}{l^2}\left(\mu^*\left\{\frac{1}{3}[(\frac{\partial u^*}{\partial x^*})^2+(\frac{\partial v^*}{\partial y^*})^2]+(\frac{\partial u^*}{\partial y^*})^2+(\frac{\partial v^*}{\partial x^*})^2\right.\right.\\ &\left.\left.+2(\frac{\partial u^*}{\partial y^*}\frac{\partial v^*}{\partial x^*})-\frac{2}{3}(\frac{\partial u^*}{\partial x^*}\frac{\partial v^*}{\partial y^*})\right\}\right)\\ \frac{\partial(\rho^* u^*\theta)}{\partial x^*}+\frac{(\partial\rho^* v^*\theta)}{\partial y^*}) &= \frac{k_0}{\rho_0 l c_p\mathrm{v}}\left(\frac{\partial k^*}{\partial x^*}\frac{\partial\theta}{\partial x^*}+k^*\frac{\partial^2\theta}{\partial x^{*^2}}+\frac{\partial k^*}{\partial y^*}\frac{\partial\theta}{\partial y^*}+k\frac{\partial^2\theta}{\partial y^{*^2}}\right)\\ &+\frac{l\Delta T}{\rho_0 c_p\mathrm{v}}q'''\\ &+\beta(\theta+T_r)\frac{p_0\Delta T^2}{\rho_0 c_p}\left(u^*\frac{\partial p^*}{\partial x^*}+v^*\frac{\partial p^*}{\partial y^*}\right)+\\ &\frac{\mu_0\mathrm{v}\Delta T}{\rho_0 c_p l}\left(\mu^*\left\{\frac{1}{3}[(\frac{\partial u^*}{\partial x^*})^2+(\frac{\partial v^*}{\partial y^*})^2]+(\frac{\partial u^*}{\partial y^*})^2+(\frac{\partial v^*}{\partial x^*})^2+\right.\right.\\ &\left.\left.2(\frac{\partial u^*}{\partial y^*}\frac{\partial v^*}{\partial x^*})-\frac{2}{3}(\frac{\partial u^*}{\partial x^*}\frac{\partial v^*}{\partial y^*})\right\}\right) \qquad (A.22)\end{aligned}$$

If we consider the non-dimensional analysis stated above, the coefficients in front of the entries can be calculated in order to compare the importance of the entries.

The material used in all analysis is air. So the properties of air should be used to calculate.

Table A.1. The ideal gas properties of air

Parameter	**Value**
μ_0	$1.7894 \times 10^{-5}(kg \quad m^{-1} \quad s^{-1})$
k_0	$0.0242(W \quad m^{-1} \quad K^{-1})$
c_p	$1006.43(J \quad kg^{-1} \quad K^{-1})$
ρ_0	$1.225(kg \quad m^{-3})$
l	0.001 (m) characteristic length of the model as the channel width
v	$0.001(m \quad s^{-1})$ characteristic velocity of the model as the inlet velocity
ΔT	$1000(^oC)$
T_r	$300(^oC)$ Ambient temperature as the reference
β	$1.02\mathbf{x}10^{-6}(K^{-1})$ for air at room temperature

Since there is no cavitation in the problem, the Euler number is taken as 1. So the p_0 value can be calculated as below:[22]

$$\begin{aligned} \mathrm{Eu} = \frac{p_0}{\rho_0 \mathrm{v}^2} &= 1 \\ \frac{p_0}{1.225 \times (0.001)^2} &= 1 \\ p_0 &= 1.225 \times 10^{-6} Pa \end{aligned}$$

As a result the non-dimesional energy equation becomes by using the coefficients:

$$\begin{aligned}\left[\frac{\partial(\rho^* u^* \theta)}{\partial x^*} + \frac{(\partial \rho^* v^* \theta)}{\partial y^*}\right] &= \underbrace{\frac{k_0}{\rho_0 l c_{p\mathrm{V}}}}_{19.628}\left(\frac{\partial k^*}{\partial x^*}\frac{\partial \theta}{\partial x^*} + k^*\frac{\partial^2\theta}{\partial x^{*2}} + \frac{\partial k^*}{\partial y^*}\frac{\partial \theta}{\partial y^*} + k\frac{\partial^2\theta}{\partial y^{*2}}\right) \\ &+ \underbrace{\frac{l\Delta T}{\rho_0 c_{p\mathrm{V}}}}_{0.811} q''' + \underbrace{\beta\frac{p_0\Delta T^2}{\rho_0 c_p}}_{1.013\times10^{-9}}\theta\cancel{\left(u^*\frac{\partial p^*}{\partial x^*} + v^*\frac{\partial p^*}{\partial y^*}\right)} \\ &+ \underbrace{\beta T_r\frac{p_0\Delta T^2}{\rho_0 c_p}}_{3.040\times10^{-7}}\cancel{\left(u^*\frac{\partial p^*}{\partial x^*} + v^*\frac{\partial p^*}{\partial y^*}\right)} + \\ &\underbrace{\frac{\mu_{0\mathrm{V}}\Delta T}{\rho_0 c_p l}}_{1.451\times10^{-5}}\cancel{\left(\mu^*\left\{\frac{1}{3}[(\frac{\partial u^*}{\partial x^*})^2 + (\frac{\partial v^*}{\partial y^*})^2]\right.\right.} \\ &\cancel{\left.\left. + (\frac{\partial u^*}{\partial y^*})^2 + (\frac{\partial v^*}{\partial x^*})^2 + 2(\frac{\partial u^*}{\partial y^*}\frac{\partial v^*}{\partial x^*}) - \frac{2}{3}(\frac{\partial u^*}{\partial x^*}\frac{\partial v^*}{\partial y^*})\right\}\right)}\end{aligned}$$

Finally, the energy equation becomes:

$$\rho c_p\frac{DT}{Dt} = div\cdot(\overrightarrow{q''}) + q''' \qquad \text{(A.23)}$$

where;

$$\overrightarrow{q''} = -k\overrightarrow{\nabla}T$$

$$q''' = -\sum\dot{\omega}_i\Delta h^0_{f,i}$$

APPENDIX B: SOLVER VERIFICATION

B.1. Comparison of the Results with the Results of FLUENT

The finite volume method is the main scheme used in famous commercial CFD solvers such as; FLUENT, STAR-CD, FLOW3D etc. [16] Consequently, one of the commercial solver, FLUENT, was picked up in order to verify the results of the solver to be created. The SIMPLE algorithm is the algorithm used to solve pressure - velocity coupled flows. So, each simulation made in FLUENT was tuned to be solved by using SIMPLE algorithm in order to be consistent in comparison.

For the sake of simplicity, the flow was assumed as incompressible and constant property which means that the density and other properties of the fluid does not change by temperature or any factor.

The velocity components on x and y direction and temperature variation can be calculated by the developed solver. The solution domain is a two dimensional channel with length/height ratio of 10. A 10 by 100 grid is used for solutions both the solver and FLUENT solutions. FLUENT solutions are given in the lower figures and figures on the top belong to the results of the own solver. The solutions are obtained for the uniform inlet velocities 0.01 and 0.001 m/s with corresponding Reynolds numbers of 684 and 68.4 respectively.

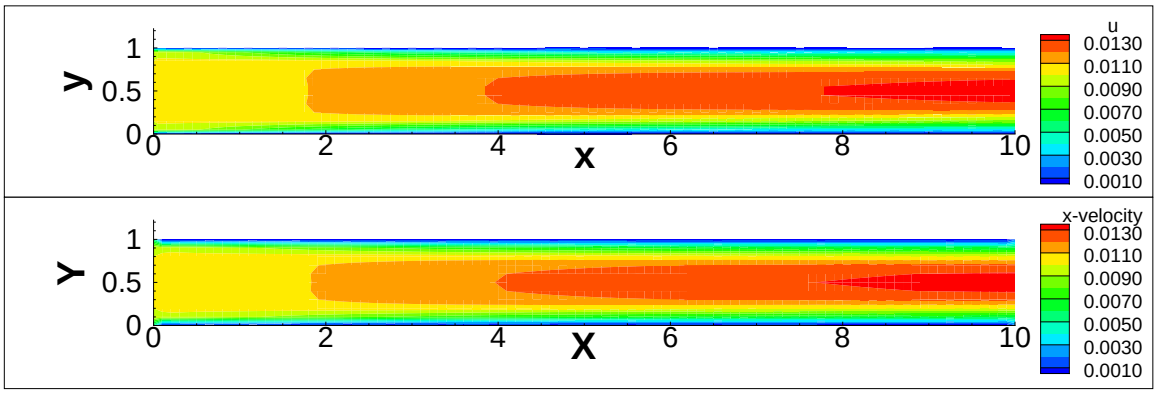

Figure B.1. x-velocity contours of duct flow with $1 \times 10^{-2} m/s$ inlet velocity

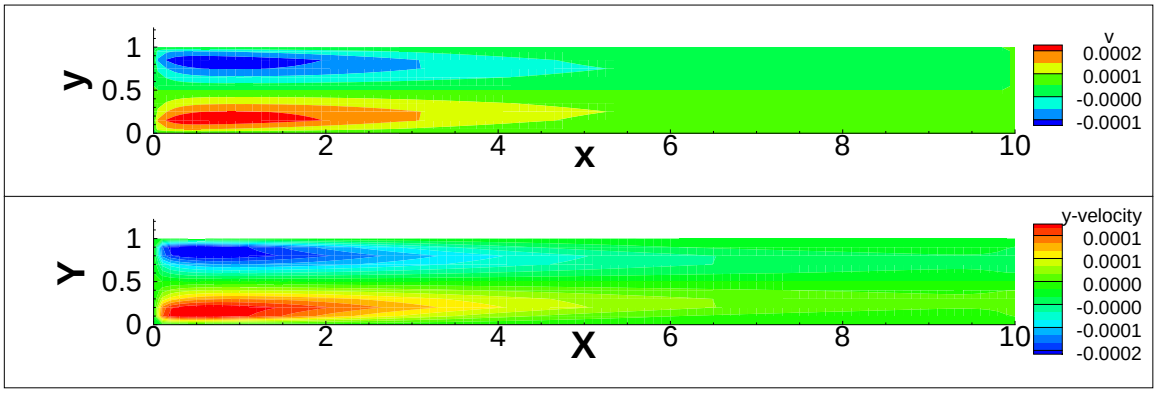

Figure B.2. y-velocity contours of duct flow with $1 \times 10^{-2} m/s$ inlet velocity

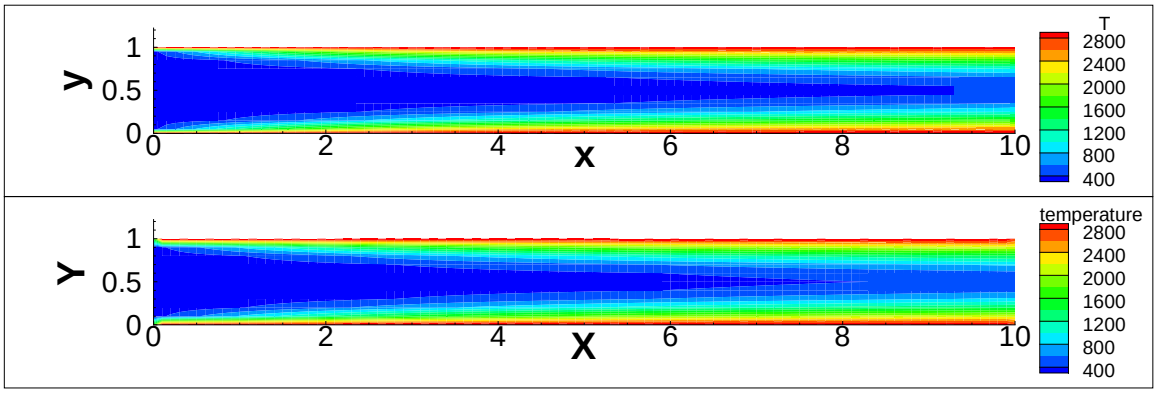

Figure B.3. Temperature contours of duct flow with $1 \times 10^{-2} m/s$ inlet velocity

The inlet velocity of the fluid is changed in order to find the capability limits of the solver and compatibility with the commercial solvers. The solutions for the inlet velocity of $1 \times 10^{-3} m/s$ is found and they are given below figures.

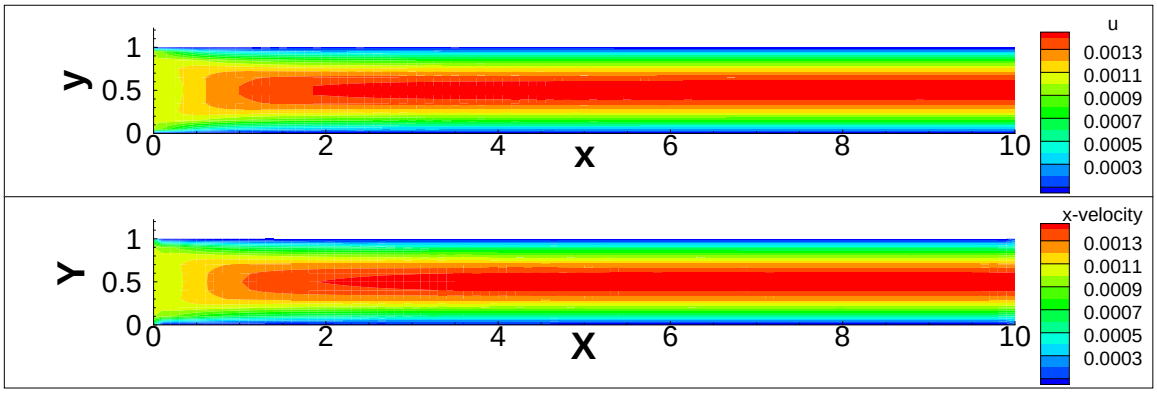

Figure B.4. x-velocity contours of duct flow with $1 \times 10^{-3} m/s$ inlet velocity

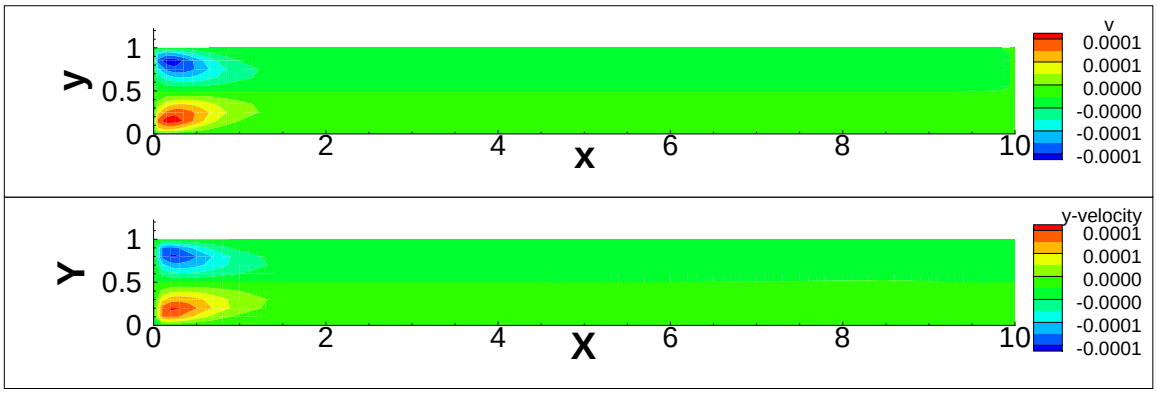

Figure B.5. y-velocity contours of duct flow with $1 \times 10^{-3} m/s$ inlet velocity

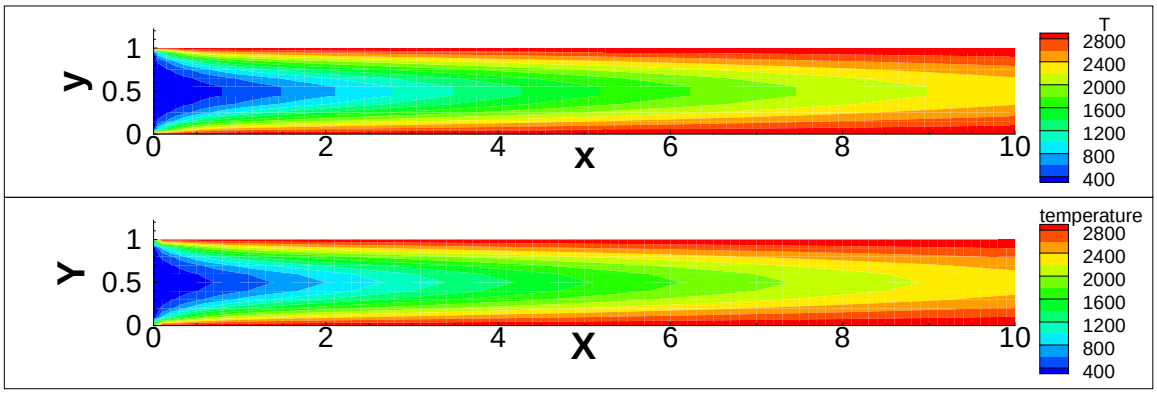

Figure B.6. Temperature contours of duct flow with $1 \times 10^{-3} m/s$ inlet velocity

B.2. Results on Different Geometries

Some calculations are made in order to develop routines solving species mass continuity equation, conjugate heat transfer condition and various geometries containing solid walls and different boundary conditions. Firstly, the solid fluid interaction is implemented by introducing the very high artificial source terms into the discretised momentum and continuity equations. So the value of the mesh point is kept fix to a prescribed value. For the velocities, pressures and later the concentration values are fix to zero at solid cells. On the other hand, high sources at solid cells are not implemented to energy equation in order the heat to propagate inside the solid domain. The basic calculations were started with a pipe flow blocked by an obstacle in the middle. The velocity and temperature contours for the case with an inlet velocity and temperature of $1 \times 10^{-3} m/s$ and 300 K and wall temperature of 3000 K are given below.

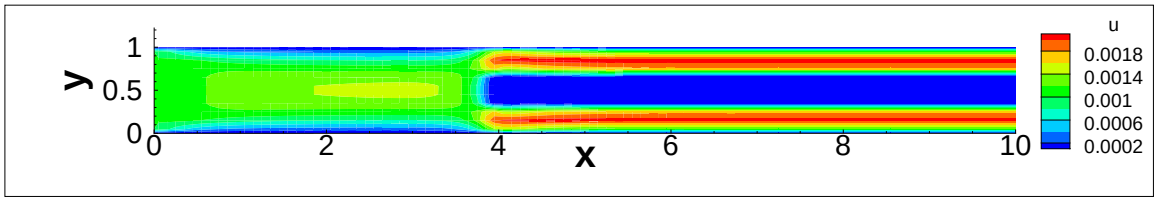

(a)

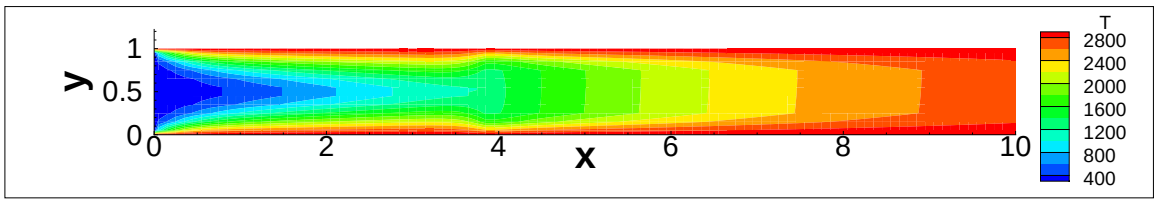

(b)

Figure B.7. x-velocity and temperature contours for pipe flow bifurcated by a solid obstacle (a) Horizontal velocity contours (b) Temperature contours

The solid inside the fluid domain concept is taken further into consideration due to the fact that the swiss-roll geometry is created by solid walls and the heat recirculation is maintained by conjugate heat transfer between fluid-solid media and conduction on solid walls. Some square shaped solid obstacles were created inside the fluid domain so that the fluid was diverted from its original direction. First a 90^o elbow is simulated. The fluid with inlet conditions of $1 \times 10^{-4} m/s$ and 300 K were flown into the domain surrounded with 1000 K constant temperature boundary condition. Secondly,

a flow whose direction is reversed by two 90^o turnings were computed. The boundary conditions of this setup were $2 \times 10^{-3} m/s$ inlet velocity and 300 K inlet temperature. The walls are kept at 1000 K constant temperature again in this simulation. The total velocity, pressure and temperature contours are given in two sets of figures below.

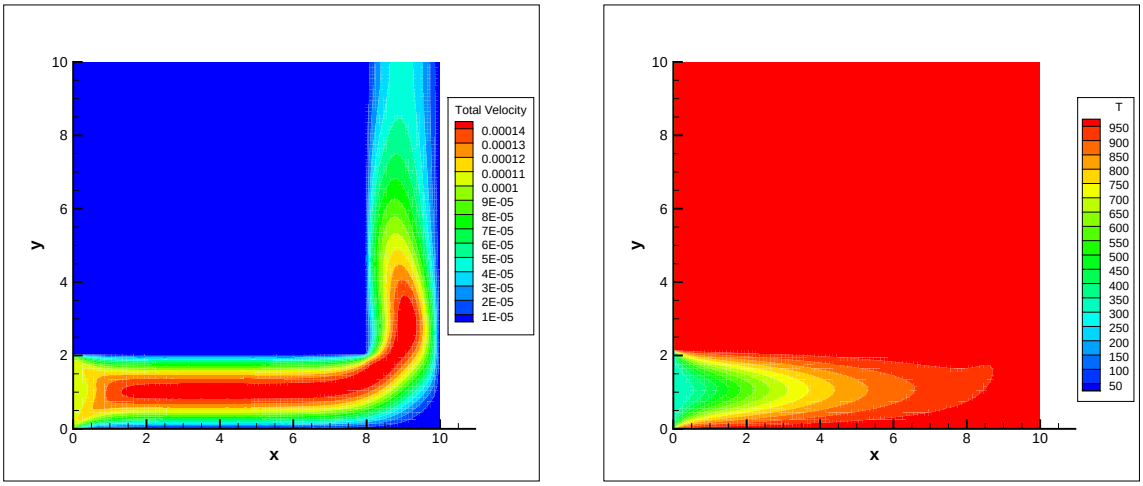

(a) (b)

Figure B.8. Total velocity, pressure and temperature contours for a 90^o elbow (a) Total velocity contours (b) Temperature contours

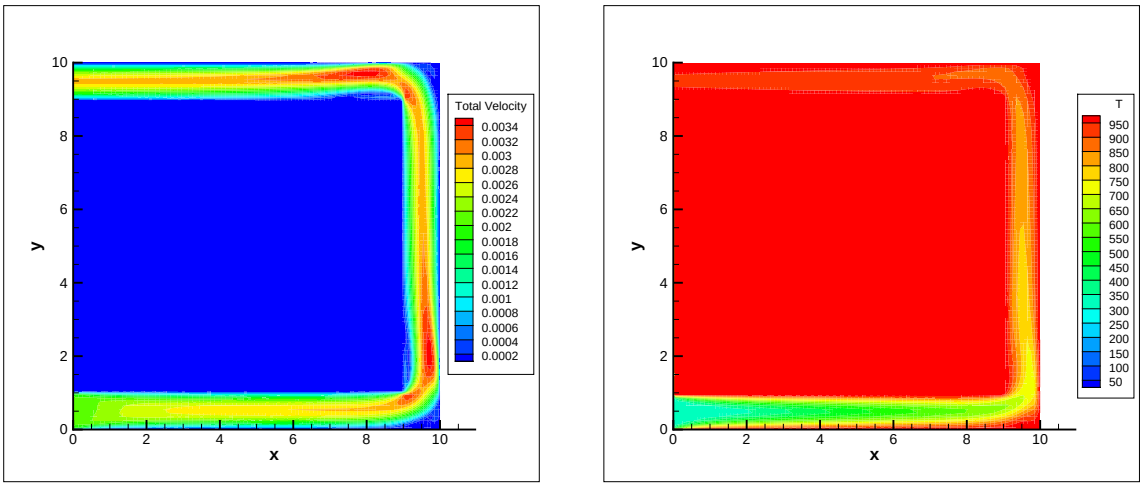

(a) (b)

Figure B.9. Total velocity, pressure and temperature contours for a U shaped tube with two 90^o turnings (a) Total velocity contours (b) Temperature contours

As the counter current type of flow and heat transfer between opposite currents are one of the main essence of the research, similar kind of flow was studied in a magnified view. The domain is cut by a solid wall and flows with same properties and

velocities ($1 \times 10^{-3} m/s$) but different temperatures(500 K and 1500 K) are let to flow. The results are quite valuable to see in heat transfer point of view. The heat leaked from high enthalpy flow to the low one. The conduction in the solid is observed. The total velocity, temperature and pressure contours are plotted in the figures.

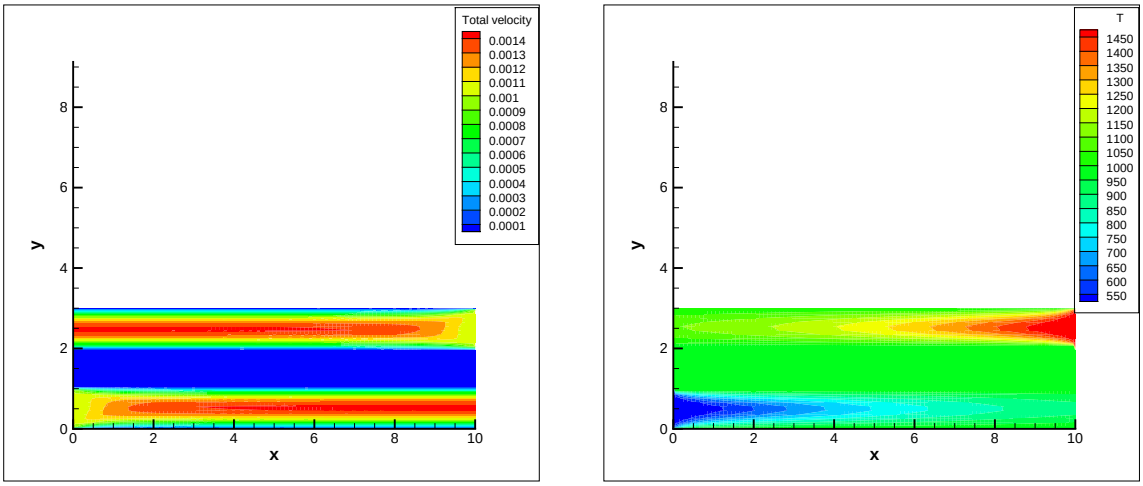

(a) (b)

Figure B.10. Total velocity, pressure and temperature contours for a counter current flow configuration (a) Total velocity contours (b) Temperature contours

The species mass continuity equation is one of the essential equations to be solved for chemically reaction flow. So a species mass continuity solver is mounted to the program. In order to have accurate and physically sound solutions one should add the ideal gas equation to the solver. Ideal gas equation not only calculates the correct density of the fluid by taking the mass fractions of the components and temperature of the fluid but also connects all equations by changing the density. So the basic test cases are run to see the abilities of these parts. A simple pipe flow whose inlet velocity and temperature are $1 \times 10^{-1} m/s$ and 300 K respectively is simulated. The composition of the fluid is set so that from upper half of the inlet only oxygen and from the lower half of the inlet only propane is let flowed. The wall temperature is 300 K. The total velocity, temperature, density, mass fraction of propane mass fraction of oxygen contours are plotted in the following set of figures.

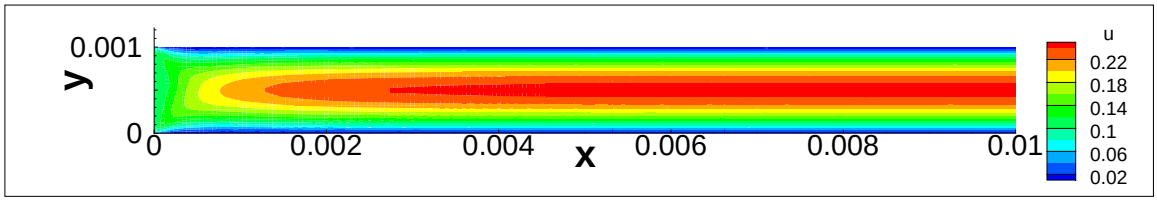

(a)

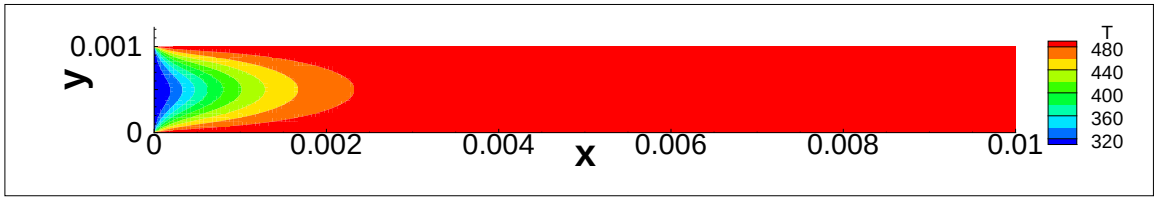

(b)

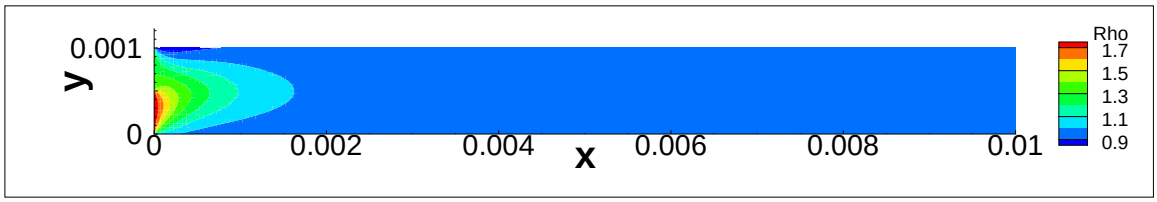

(c)

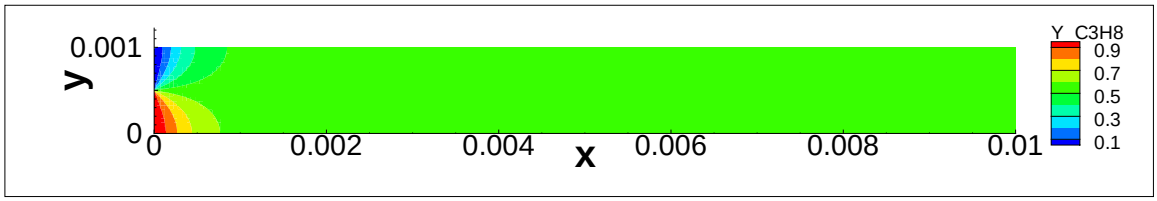

(d)

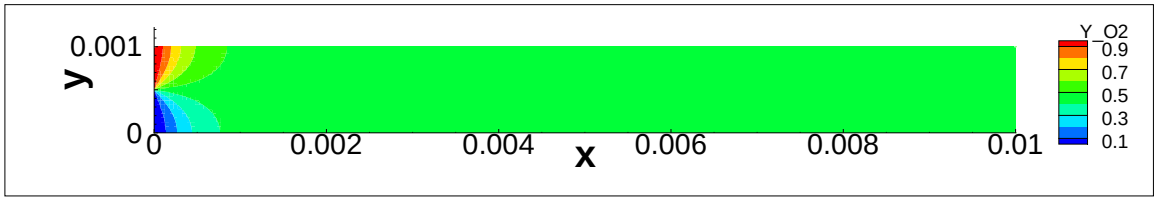

(e)

Figure B.11. Total velocity, temperature, density and mass fraction contours for a pipe flow (a) Total velocity contours (b) Temperature contours (c) Density contours (d) Mass fraction of C_3H_8 contours (e)Mass fraction of O_2 contours

The most important boundary condition for species mass continuity equation is impermeable wall boundary condition. This is also implemented to the solver for later use. The ability of that is examined by flow in a small U tube with outer and inner solid walls. The flow conditions of the test case are $1 \times 10^{-2} m/s$ inlet velocity, 300

K inlet temperature and half propane and half oxygen stream by means of inlet area. The maximum mass fraction error is 1.6×10^{-3}. The total velocity, pressure, density, mass fraction of propane mass fraction of oxygen and mass fraction error values are plotted below.

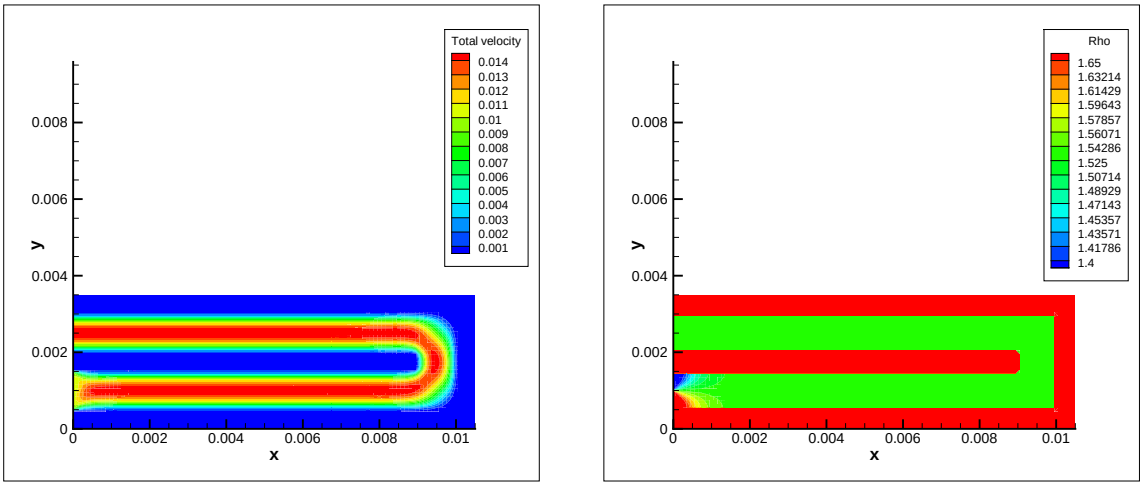

(a)

(b)

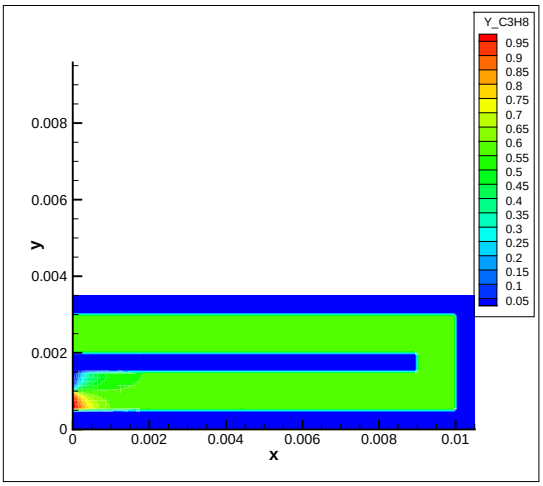

(c)

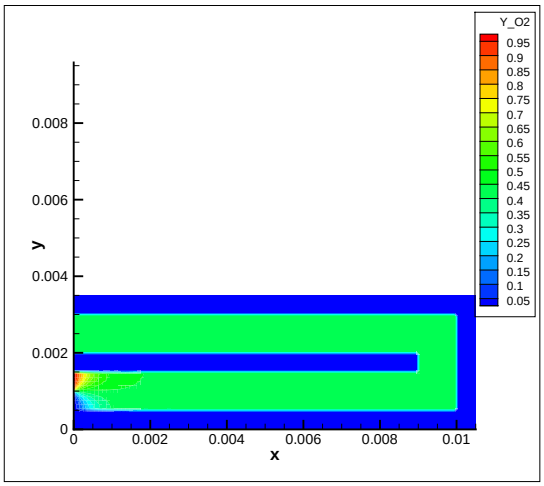

(d)

Figure B.12. Total velocity, pressure, density, mass fractions and mass fraction error contours for a U-tube flow (a) Total velocity contours (b) Density contours (c) Mass fraction of C_3H_8 contours (d)Mass fraction of O_2 contours

REFERENCES

1. D Ronney, Combustion and Flame 135 (2003) 421-439

2. D C Kyritsis, S Roychoudhury, C S McEnally, L D Pfefferle, A Gomez, Experimental Thermal and Fluid Science 28 (2004) 763-770

3. S A Lloyd, F J Weinberg, Nature 251 (1974) 47-49

4. S A Lloyd, F J Weinberg, Nature 257 (1975) 367-370

5. A R Jones, S A Lloyd, F J Weinberg, Proc. R. Soc. Lond. 360 (1978) 97-115

6. J Ahn, C Eastwood, L Sitzki, P D Ronney, Proceedings of the combustion Institute 30 (2005) 2463-2472

7. M Chen, J Buckmaster, Combustion Theory Modeling 8 (2004) 701-720

8. L Sitzki, K Borer, E Schuster, P Ronney, S Wussow, The Third Asia- Pacific Conference on Combustion (2001) Seul Korea

9. N I Kim, S Kato, T Kataoka, T Yokomori, S Maruyama, T Fujimoro, K Maruta, Combustion and Flame 141 (2005) 229-240

10. J Vican, B F Gajdeczko, F L Dryer, D L Milius, I A Aksay, Proceedings of the Combustion Institute 29 (2002) 909-916

11. C K Westbrook, F L Dryer, Prog. Energy Combust. Sci. 10 (1984) 1-57

12. K K Kuo, Principles of Combustion, John Wiley & Sons Inc., 2005

13. C K Westbrook, F L Dryer, Combustion Science and Technology. Sci. 27 (1981) 31-43

14. G L Borman, K W Ragland, Combustion Engineering, McGraw-Hill, 1998

15. TRANSPORT Core Utility Manual, Reaction Design, 2003

16. H K Versteeg, W Malalasakera, An introduction to computational fluid dynamics, Longman Scientific and Technical, First ed., 1995

17. H K Versteeg, W Malalasakera, An introduction to computational fluid dynamics, Pearson Education Limited, Second ed., 2007

18. S V Patankar, Numerical Heat Transfer and Fluid Flow, Hemisphere Pub. Corp., 1980

19. S V Patankar, D B Spalding, International Journal of Heat Mass Transfer 15 (1972) 1787-1806

20. C H Kuo, Numerical Modeling Of Non-Adiabatic Heat Recirculating Combustors, Ph.D. Thesis, University of Southern California, 2006

21. L C Burmeister, Convective Heat Transfer, John Wiley & Sons, Inc, 1993

22. B R Munson, D F Young, T H Okiishi, Fundamentals of Fluid Mechanics, John Wiley & Sons, Inc., Fourth ed., 2002